

# Diversity You Can Actually Measure: A Fast, Model-Free Diversity Metric for Robotics Datasets

Sreevardhan Sirigiri<sup>1</sup> Nathan Samuel de Lara<sup>2</sup> Christopher Agia<sup>3</sup> Florian Shkurti<sup>2,4</sup> Fabio Ramos<sup>1,5</sup>

**Abstract**—Robotics datasets for imitation learning typically consist of long-horizon trajectories of different lengths over states, actions, and high-dimensional observations (e.g., RGB video), making it non-trivial to quantify diversity in a way that respects the underlying trajectory structure and geometry. We extend Shannon and von Neumann entropy to this setting by defining signature transform-based entropy on the Gram matrix of a signature kernel over demonstrations, yielding entropy and diversity metrics that operate directly on the demonstration dataset. Building on these metrics, we study how dataset diversity affects generalization performance in robot imitation learning and propose a simple, model-free way to curate diverse demonstrations. We introduce FAKTUAL (FAst trajectory Kernel enTropy cUration for imitation Learning), a data curation algorithm that selects a subset of demonstrations maximizing entropy given a subset-size budget. FAKTUAL is fully model-free, requires no access to the imitation policy or rollouts, and adds negligible overhead relative to policy training. We evaluate our approach on image and state-based RoboMimic and MetaWorld benchmarks, as well as four real-world manipulation tasks. Across tasks and architectures, diversity-aware curation with FAKTUAL consistently improves downstream success rates over random selection, while being substantially more computationally efficient compared to recent robot data curation methods. Our results suggest that the entropy of demonstration datasets is a practical tool for understanding and improving dataset diversity in robot imitation learning.

## I. INTRODUCTION

Although many of the most prominent advances in deep learning have been driven by architectural innovations and increases in dataset scale, the diversity of the training data is also a crucial determinant of model performance. Diversity of datasets is a desirable criterion across many areas of machine learning, including dataset curation, generative modeling, reinforcement learning, active learning, and decoding algorithms [23]. Robotics, in particular imitation learning (IL), is no exception to this [53, 7, 30, 24, 68]. Recent works on large and (anecdotally) diverse datasets have been a central driver of scaling in robot imitation learning [53, 35, 9, 82, 51, 37, 7, 30].

Despite growing interest in leveraging large robot datasets, there remains no widely accepted measure of diversity for such data. Moreover, quantifying diversity in robotics datasets in a principled way is difficult and non-trivial. This challenge stems from two main reasons: (1) demonstrations are often

long-horizon trajectories/paths of varying lengths and consist of multiple modalities such as states, actions/control inputs and high-dimensional sensory observations (e.g., video); and (2) a diversity metric requires a mathematical notion of similarity between demonstrations that goes beyond pointwise distance and instead respects the underlying trajectory structure and geometry.

In this work, we leverage the signature kernel to define a notion of diversity. The signature transform and its associated signature kernel [42, 13] provide a principled way to represent and compare paths/trajectories of variable length while preserving important aspects of their geometric and sequential structure. Hence, the signature kernel induces a similarity measure that respects trajectory structure and geometry rather than relying on pointwise distances. Prior work has demonstrated that signature-kernel-based methods discriminate between robotic paths in applications such as trajectory optimization, path planning, and ergodic search [4, 70]. Additionally, the signature kernel’s mathematical properties are meaningful for robot trajectories and can provide a solution for the challenges mentioned earlier.

In addition to spanning a diverse and broad set of behaviors and states, a dataset must also provide sufficient *coverage* around those behaviors and states, i.e., enough local “*density*” of demonstrations for a reliable IL policy rather than merely observe isolated (and possibly outlying) trajectories. Demonstration *quality* is likewise essential: a dataset can hinder learning if large portions of the data are suboptimal or inconsistent [44]. In this sense, quality, diversity, density are complementary properties that jointly determine downstream policy performance.

Curating datasets using principled diversity metrics as a first-class signal remains largely unexplored, and existing pipelines often do not explicitly preserve diversity during selection. Moreover, when overall dataset quality is already high across demonstration trajectories, the importance of diversity and balanced coverage/density (i.e., a uniform coverage of states and behaviors) can become even more pronounced [54]. In fact, recent work has devoted considerable attention to data curation for improving the quality of robot imitation learning datasets [40, 27, 11, 12, 3]. A largely successful approach is to retain only demonstrations judged to be beneficial according to a heuristic, *task-agnostic* notion of quality, producing a smaller dataset curated offline [27]. A limitation of several curation approaches (e.g., [27, 12, 11, 3]) is that they typically rely on training an auxiliary model to compute heuristic scores, often incurring large upfront costs comparable to training the target policy itself. Moreover, due to the computational intensity

<sup>1</sup>The University of Sydney. <sup>2</sup>University of Toronto. <sup>3</sup>Stanford University. <sup>4</sup>Allen Institute for Artificial Intelligence. <sup>5</sup>NVIDIA, USA

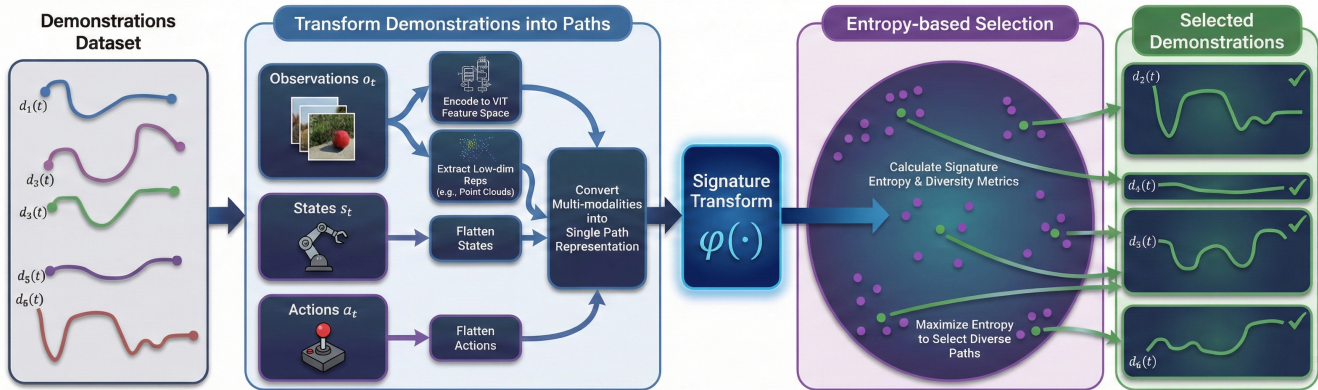


Fig. 1: A graphical depiction of FAKTUAL. First, for each demonstration in the dataset, we embed the observations—specifically, the RGB images—into a ViT feature space, or alternatively extract low-dimensional representations of the objects of interest (e.g., point clouds) from the images. We then flatten any additional modalities present in the demonstrations, such as states and actions, if required, so that each demonstration can be represented as a paths or trajectories in space (detailed steps can be found in Appendix A). Using these path representations, we compute signature-based entropy and diversity metrics, which we then use to select a subset of the dataset that maximizes the entropy or diversity.

of these approaches, they are often best applied to smaller, task-specific fine-tuning datasets (e.g., post-training) than to large-scale multi-task datasets (e.g., pre-training). However, if diversity can be computed cheaply and reliably, it can provide a practical dataset-level signal for curation without requiring an additional learned scoring model and could be applied to large datasets. Such a curation approach would be complementary to quality based curation, meaning the methods could be combined to create datasets with positive quality and diversity properties.

Furthermore, while diversity is not itself a direct measure of task success, it can nevertheless provide an explicit dataset-level signal that relates the composition of the training set to downstream performance. Indeed, we show later in the paper that demonstration diversity correlates well with policy success rate, suggesting that diversity can serve as a practical and informative criterion for curation.

**Contributions:** Our main contributions are two-fold. (1) We compute Shannon entropy and von Neumann entropy on the eigenvalues of the signature kernel, providing a computationally cheap and principled way to measure the entropy and diversity of robotics datasets; our construction explicitly incorporates states, actions, videos and other modalities when defining this entropy-based diversity metric. (2) We propose a data curation strategy, **FAKTUAL** (FAst trajectory Kernel enTropy cUration for imitation Learning) grounded in this new notion of entropy and diversity, selecting a subset of the full dataset that maximizes entropy or diversity which can be used to remove redundant demonstrations making the dataset more uniform in the demonstrations (or trajectory) modes i.e., states and behaviors. Our data curation strategy is completely model-free, requires no information about the imitation learning policy being trained or its rollouts, and depends solely on the dataset itself. We show empirically that diversity-aware curation, though a heuristic, improves policy performance.

## II. RELATED WORK

a) *Dataset Diversity in Robotics:* Shi et al. [68] consider

a multi-task setting and show that: (1) task diversity proves more critical than per-task demonstration quantity; (2) multi-embodiment pre-training data is not strictly necessary for cross-embodiment transfer—models trained on high-quality single-embodiment data can transfer efficiently to different platforms and exhibit more favorable scaling behavior during fine-tuning than multi-embodiment pre-trained models; and (3) expert diversity, stemming from individual operational preferences and stochastic variability in human demonstrations, can confound policy learning, with velocity multimodality (same action done slower/faster) being harmful to the performance and spatial multimodality being beneficial for performance. D3IL [31] designs tasks with explicitly defined multiple successful behaviors and multiple human demonstrators, and evaluates IL algorithms using behavior entropy alongside success rate. They show that some advanced methods (especially diffusion-based transformer policies) can achieve both high diversity and high success. Chi et al. [15] collect demonstrations “in the wild” across diverse locations and object variants and shows that a single policy trained on this heterogeneous dataset generalizes to unseen environments and objects, including out-of-distribution settings (e.g., novel lighting, textures, surfaces).

b) *Data Curation in Robotics:* Recent work has attempted to explicitly quantify the value of individual demonstrations for data curation [40, 27, 11, 12]. Hejna et al. [27] estimates demonstration quality heuristic based on mutual information by training a VAE, and hence does not explicitly incorporate policy performance. However, this method can only filter existing data. Chen et al. [11] on the other hand train classifiers to distinguish successful from failed rollouts across policy checkpoints. In contrast to these methods, Agia et al. [3] directly quantify the causal influence of each demonstration on the policy’s expected return, yielding a signal that does not require access to both successes and failures. DataMIL [18] applies datamodels to select from large multi-task datasets using an offline metric. SCIZOR [81] is a self-supervised data curation approach to filter out suboptimal data, which hinder

learning with undesirable actions, and redundant data, which dilute training with repetitive patterns.

c) *The signature (transform) and its corresponding kernel* [42, 13]: have proven to be highly effective in robotics and deep learning when data is naturally represented as a continuous paths or trajectories [13, 8, 77, 52]. Prior work has leveraged signature-based representations for diverse objectives, including motion planning in robotics where the signature kernel was used as similarity function between trajectories to produce diverse solutions for manipulation tasks [4], human action recognition [77], and trajectory following or stabilization via signature methods [52]. Signatures have also been applied to data-driven control, where trajectory information is encoded compactly to support learning and control design [65].

Friedman and Dieng [23] introduce the Vendi score which uses kernels to measure the diversity of a dataset. Subsequent works show that Vendi scores can be extended to measure information gain [50], and improve retrieval augmented generations [58]. We extend the idea underlying the Vendi score to the robotic domain using Signature transforms and the Signature kernel. We also connect the Vendi score to Von Neumann and Shannon entropy under the Signature kernel.

In Appendix H we have a more complete discussion of related works that focus on dataset diversity in non-robotics machine learning applications.

### III. PROBLEM STATEMENT

The goal of this work is to characterize the relationship between demonstration dataset diversity and model performance in closed-loop robotic imitation learning, and leverages this relationship to motivate a diversity-based pruning method. Accordingly, we consider a finite-horizon Decision Process  $\langle \mathcal{S}, \mathcal{A}, \mathcal{T}, R, \rho_0, \mathcal{O}, \dots \rangle$  with state space  $\mathcal{S}$ , action space  $\mathcal{A}$ , transition model  $\mathcal{T}$ , reward function  $R$ , initial state distribution  $\rho_0$ , observation space  $\mathcal{O}$  and finite horizon  $T$ . We train a policy  $\pi_\theta$  by minimizing a behavior cloning (BC) objective, i.e.,

$$\theta = \arg \min_{\theta'} \left\{ \mathcal{L}(\theta'; \mathcal{D}) := \frac{1}{|\mathcal{D}|} \sum_{d_i \in \mathcal{D}} \frac{1}{T_i} \sum_{(s,a) \in d_i} \ell(s, a; \pi_{\theta'}) \right\},$$

using a dataset of demonstrations  $\mathcal{D} = \{d_1, \dots, d_n\}$ . Each demonstration  $d_i = ((s_i(0), a_i(0), o_i(0)), \dots, (s_i(T_i), a_i(T_i), o_i(T_i)))$  is a state-action-observation trajectory in which the robot successfully completes the task. We treat a trajectory  $\tau = (s(0), a(0), \dots, s(T))$  as either a *success* or a *failure*, corresponding to binary returns  $R_i(t) = 1$  and  $R_i(t) = -1$ , respectively for some  $t \in T$ .

In imitation learning, we train the policy  $\pi_\theta$  to match the distribution of successful behaviors in  $\mathcal{D}$  (rather than directly maximizing its expected return  $J(\pi_\theta) := \mathbb{E}_{p(\tau|\pi_\theta)}[R(\tau)]$ ). As a consequence, the policy’s performance is tightly coupled to the demonstration data composition—and not solely to validation losses, model capacity, or bias–variance trade-offs [3]. This dependence makes systematic performance improvement challenging. Recent work highlights that merely scaling demonstration collection can produce datasets with

redundancy and behaviors that degrade policy performance, despite having  $R(d_i) = 1$  for all demonstrations  $d_i \in \mathcal{D}$  [5].

In this paper, the problem we are focused on is finding a measure of dataset diversity or information content  $f(D) \in \mathbb{R}_{\geq 0}$  such that  $f(\cdot)$  correlates positively with the success rate of a policy trained on  $D \subseteq \mathcal{D}$ ,  $\mathcal{J}(\pi_D)$ . Given such a measure  $f$ , we hope to use  $f$  for finding data subsets  $D \subseteq \mathcal{D}$  where  $f(D) \approx f(\mathcal{D})$  and hence  $\mathcal{J}(\pi_D) \approx \mathcal{J}(\pi_{\mathcal{D}})$ .

## IV. BACKGROUND & PRELIMINARIES

### A. Signature Transform and Signature Kernel

Informally, the signature transform of a trajectory can be viewed as analogous to a Fourier series: it represents a path of variable length as a countably infinite sequence of features capturing its geometric and temporal structure. We now introduce the signature transform of a path/trajectory and its corresponding kernel:

**Definition 1. (Informal) Signature (transform) of a path** [63]. *Let  $x : I \rightarrow \mathbb{R}^d$  be a continuous path on an interval  $I \subset \mathbb{R}$ . For any subinterval  $[s, t] \subset I$ , the signature of  $x$  over  $[s, t]$  is the sequence*

$$\varphi(x)_{s,t} = \left( 1, \int_{s < u_1 < t} dx(u_1), \dots, \int_{s < u_1 < \dots < u_k < t} dx(u_1) \otimes \dots \otimes dx(u_k), \dots \right), \quad (1)$$

where  $\otimes$  denotes the (classical) tensor product. This family of iterated integrals encodes salient information about the path and is invariant to reparameterization (i.e.,  $\varphi(x) = \varphi(x \circ \theta)$  for any reparameterization  $\theta$ ).

The path signature may be viewed as a canonical linear embedding of a multivariate path into an (infinite) series of iterated integrals. It is injective on the class of non-tree-like paths (in practice, non-tree-likeness is typically enforced by appending a monotone “time” coordinate). The signature also obeys a *time-reversal duality*:  $\varphi(x)_{a,b} \otimes \varphi(\overleftarrow{x})_{a,b} = 1$ , where 1 is the unit element and  $\overleftarrow{x}(t) = x(a + b - t)$ .

**Definition 2. (Informal) Signature Kernel.** *Let  $I = [u, u']$  and  $J = [v, v']$  be intervals, and let  $x \in \mathcal{C}^1(I, \mathbb{R}^d)$  and  $y \in \mathcal{C}^1(J, \mathbb{R}^d)$  be paths. The signature kernel  $k^{sig}(x, y) : I \times J \rightarrow \mathbb{R}$  is defined as follows*

$$k_{s,t}^{sig}(x, y) = \langle \varphi(x)_s, \varphi(y)_t \rangle,$$

where  $\varphi(x)_s$  and  $\varphi(y)_t$  denote the signatures of  $x$  and  $y$  over  $[u, s]$  and  $[v, t]$ , respectively.

In practice, the signature kernel can be well approximated via the *truncated signature transform* at level  $L \in \mathbb{N}$  (see Appendix B),

$$\varphi_{s,t}^L(x) = \left( 1, \int_{s < u_1 < t} dx(u_1), \dots, \int_{s < u_1 < \dots < u_L < t} dx(u_1) \otimes \dots \otimes dx(u_L) \right). \quad (2)$$

The work of Kiraly and Oberhauser [38] and Tóth et al. [74] provide efficient procedures for computing the truncated signature transform and its induced kernel using dynamic programming, and for approximating it with random Fourier features (see Appendix C), respectively. Moreover, the untruncated signature transform and its kernel can be computed via a *kernel trick* (see Appendix B) introduced by Salvi et al. [63].

## B. Entropy

Entropy has long been used as a measure of randomness in a system across many fields, including physics, ecology, signal processing, information theory, and machine learning. It is often interpreted as the amount of information required to “describe” a system—the greater the randomness, the more information is needed to fully characterize it.

In statistical physics, the (Gibbs) entropy [25] is defined as  $H_{\text{gibbs}} = -k_B \sum_i p_i \ln p_i$ , where  $p_i$  denotes the probability of each microscopic configuration  $x$  of a system that is consistent with the macroscopic constraints (such as total energy, volume, and number of particles), and  $k_B$  is Boltzmann’s constant. Shannon’s entropy [66] generalizes the Gibbs entropy, leading to the definition of information entropy as

$$H_{\text{shannon}}(X) = - \sum_{x \in \mathcal{X}} p(x) \ln p(x), \quad (3)$$

where  $X$  is a discrete random variable with support  $\mathcal{X}$  and  $p(x) = \mathbb{P}(X = x)$ . In general, the Shannon entropy measures the average uncertainty associated with the outcome of  $X$ . In other words, the higher the Shannon entropy, the more uniform and spread out the distribution is.

1) *Von Neumann Entropy*: The *von Neumann entropy* [49, 21] is the quantum analogue of Shannon entropy: it extends the notion of information-theoretic uncertainty from classical probability distributions to quantum states. Speaking very informally, the von Neumann entropy is defined as

$$H_{\text{von neumann}} = -\text{Tr}(\rho \ln \rho), \quad (4)$$

where  $\rho$  is the density matrix, whose rows and columns correspond to the (quantum) states of the systems. The diagonal entries capture the probabilities of the system being in each state, while the off-diagonal entries reflect the “mixing” or coherence between different states.

## V. MEASURING DIVERSITY OF DATASETS IN ROBOTICS

The definition of Shannon entropy, given in Eq. (3), requires a probability distribution (or a tractable method of computing the probability distribution), which is not feasible in many robotics contexts. Our goal is to establish a diversity metric that depends solely on the samples under evaluation. This necessitates the definition of a similarity function over the samples. We can use the signature kernel for such a similarity function.

The signature of a trajectory is invariant under reparameterization, i.e., it does not change when the same geometric path is traversed at a different speed. This invariance effectively filters out the complicated, infinite-dimensional group of symmetries.

Moreover, the collection of linear functionals on the signature forms an algebra under pointwise multiplication and is rich enough to separate points [1]. Consequently, by the *Stone–Weierstrass* theorem [60], for any compact set  $\mathbf{C}$  of continuous paths with bounded variation, these linear functionals are dense in the space of continuous real-valued functions on  $\mathbf{C}$  [43]. Together, these results motivate the signature as a powerful feature map for representing demonstrations in robotics, once demonstrations are encoded as paths or trajectories.

We convert each demonstration into a (multivariate) path by (i) embedding raw visual observations at each time step into a fixed-dimensional vector (e.g., a ViT embedding, or a low dimensional representation) and then (ii) concatenating it with the per-timestep robot state and action to form a trajectory  $X_i(t)$  over time. Alternatively, we can treat each modality (i.e., states, actions, observations etc.) as its own path and combine them via a convex combination of the corresponding signature kernels (see Appendix A for details).

We can now construct a form of entropy that relies only on the evaluated samples for measuring diversity.

**Definition 3** (Signature Shannon Entropy). *Let  $k^{\text{sig}}$  be the signature kernel,  $d_1, d_2, \dots, d_n \in \mathcal{D}$  be a set of demos, and  $K^{\text{sig}} \in \mathbb{R}^{n \times n}$  denote the normalized kernel matrix produced by  $k^{\text{sig}}$  with entries  $K_{i,j}^{\text{sig}} = k^{\text{sig}}(d_i, d_j)$  and  $K_{i,i}^{\text{sig}}(d_i, d_i) = 1$ . The signature Shannon entropy is given by*

$$H_{\text{shannon}}^{\text{sig}}(d_1, d_2, \dots, d_n) = - \sum_{\lambda_i \in \Lambda} \lambda_i \ln \lambda_i, \quad (5)$$

where  $\Lambda$  is the set of eigenvalues of  $K^{\text{sig}}/n$ .

The eigenvalues of  $K/n$  are nonnegative, since  $k^{\text{sig}}$  is positive semidefinite, and they sum to one, as each diagonal entry of  $K/n$  equals  $1/n$ . Consequently, Shannon entropy is well-defined.

**Definition 4** (Signature von Neumann Entropy). *Consider the same notation used in Definition 3. The signature von Neumann entropy is defined as*

$$H_{\text{von neumann}}^{\text{sig}}(d_1, d_2, \dots, d_n) = -\text{Tr} \left( \frac{K^{\text{sig}}}{n} \ln \frac{K^{\text{sig}}}{n} \right). \quad (6)$$

Remarkably, it turns out that  $H_{\text{shannon}}^{\text{sig}} = H_{\text{von neumann}}^{\text{sig}}$ , see Appendix I and [23]. Exponentiating this Shannon/von Neumann entropy, defined using any positive definite kernel, gives the effective rank of the corresponding kernel matrix (see [59]), which can be used to define the Vendi score, a diversity metric introduced by Friedman and Dieng [23].

The entropy of a dataset reflects how uniformly random and well-distributed the samples are. Another useful metric is the volume spanned by the samples (i.e., the demonstrations), which can be measured using

$$\Delta(d_1, d_2, \dots, d_n) := \det(K^{\text{sig}}), \quad K_{i,j}^{\text{sig}} = k^{\text{sig}}(d_i, d_j).$$

<sup>0</sup> The kernel  $k(d_i, d_j)$  can be viewed as a similarity score between demonstrations  $d_i$  and  $d_j$ . In particular, for a normalized

<sup>0</sup>Technically,  $\Delta(d_1, \dots, d_n)$  gives the volume of the parallelotope, spanned by the feature embeddings of the samples in the RKHS induced by  $k$ .

kernel (i.e., with  $k(d_i, d_j) \leq 1$  and  $k(d_i, d_i) = 1$ ),  $k(d_i, d_j) \rightarrow 1$  as  $d_i \rightarrow d_j$ ,  $k(d_i, d_j) \rightarrow 0$  as  $\|d_i - d_j\| \rightarrow \infty$ . Given a set of trajectories, their diversity may be assessed by constructing the Gram matrix  $K \in \mathbb{R}^{n \times n}$ ,  $K_{ij} = k(d_i, d_j)$ ,  $K_{ii} = 1$ , and evaluating its determinant. In particular,  $\det(K) \rightarrow 0$  if  $d_i \rightarrow d_j$  for any  $i \neq j$ ,  $\det(K) \rightarrow 1$  as  $\|d_i - d_j\| \rightarrow \infty$  for all  $i \neq j$ , thus yielding another principled measure of diversity.

## VI. DATA CURATION WITH SIGNATURE DIVERSITY METRICS

We first introduce a set of definitions:

**Definition 5** (Signature-entropy-maximizing  $m$ -subset). Consider the notation introduced in Definition 3 and let Signature Entropy  $H := H_{shannon}^{sig} = H_{von\ neumann}^{sig}$ . The Signature-entropy-maximizing  $m$ -subset  $(\hat{D}_m^{entropy})$  is defined as,

$$H(\hat{D}_m^{entropy}) \geq H(D_m), \quad \forall D_m \subseteq \mathcal{D}, |D_m| = m. \quad (7)$$

**Definition 6** (Signature-determinant-maximizing  $m$ -subset). Consider the notation introduced in Definition 3, and then Signature-determinant-maximizing  $m$ -subset  $(\hat{D}_m^{det})$  is defined as,

$$\Delta(\hat{D}_m^{det}) \geq \Delta(D_m), \quad \forall D_m \subseteq \mathcal{D}, |D_m| = m. \quad (8)$$

In general, finding the signature-determinant-maximizing  $m$ -subset or signature-entropy-maximizing  $m$ -subset reduces to a well-known NP-Hard problem from combinatorial optimization called maximum coverage (a.k.a. max- $k$ -cover) [34, 36]. Hence, one can only obtain an approximate solution in polynomial time. See Appendix E for algorithms to approximate such a set. Typically these algorithms employ a greedy strategy by iteratively adding demonstrations to the set that maximally increase the entropy or determinant.

**Data Curation Strategy.** Our data curation strategy is straightforward: to curate a dataset of size  $m$ , we select the (approximate) signature-entropy-maximizing  $m$ -subset of  $\mathcal{D}$ . This choice is justified because, in practice, the signature entropy  $H$  exhibits diminishing returns as additional data points are added. Consequently, beyond a certain subset size, including more data points only marginally increases the entropy, which eventually approaches saturation and asymptotes (see Figure 2). Hence, a properly curated subset by maximizing the entropy can achieve nearly the same entropy (or the "information content") as the full dataset while using far fewer demonstrations while encouraging uniform coverage/density.

Selecting the signature-entropy-maximizing  $m$ -subset primarily promotes uniform randomness, but it may overlook certain extreme data points. In practice, it can be beneficial to include such points (except when they are extremely poor and should have been filtered out beforehand). Therefore, an objective that maximizes the volume of the subset, such as det  $K$ , can be useful.

To curate a dataset of size  $m$ , we proceed as follows:

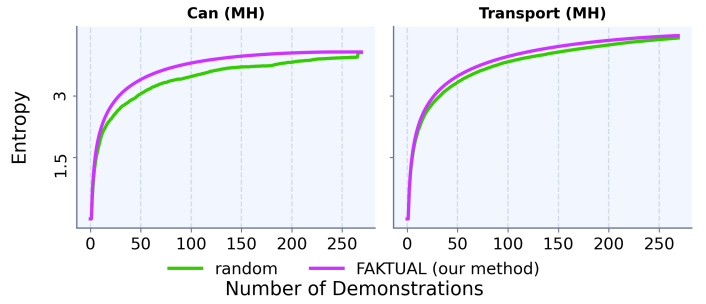


Fig. 2: Entropy vs Number of Demonstrations. In the Can task, the entropy saturates quickly and approaches an asymptote. In contrast, the Transport task entropy does not saturate over the range shown, indicating that the Transport task is more diverse (at least as discriminated by the signature entropy) and each demonstration contributes almost equally to the entropy, hence we see a weaker separation between the random and FAKTUAL lines. Note that the exact value of entropy varies greatly with the chosen kernel bandwidth; hence for brevity we choose a bandwidth of 1.0 for this figure.

- 1) Fix a proportion parameter  $p \in [0, 1]$ . In practice, a suitable range for  $p$  is between 0.5 and 0.9.
- 2) Select the (approximate) signature-entropy-maximizing subset of size  $mp$ :  $\hat{D}_{mp}^{entropy} \subseteq \mathcal{D}$ ,  $|\hat{D}_{mp}^{entropy}| = mp$ .
- 3) From the remaining samples, select the (approximate) signature-determinant-maximizing subset of size  $m(1-p)$ :  $\hat{D}_{m(1-p)}^{det} \subseteq \mathcal{D} \setminus \hat{D}_{mp}^{entropy}$ ,  $|\hat{D}_{m(1-p)}^{det}| = m(1-p)$ .
- 4) Finally, return the union of the sets  $\hat{D}_{mp}^{entropy} \cup \hat{D}_{m(1-p)}^{det}$ .

We provide details of the algorithms to compute the subset in Appendix E.

## VII. EXPERIMENTS AND RESULTS

In this section, we present results to empirically demonstrate the effectiveness and applicability of the methods discussed above in a variety of simulated and real experiments (their exact setup can be found in Appendix F). Specifically, we are interested in addressing: (1) The success rate versus the size of the curated dataset of size  $m$  for various tasks. (2) The success rate of our method compared to other baseline data curation strategies. (3) The effect of diversity on the success rate.

### A. Simulated Experiments

We evaluate on simulation tasks from RoboMimic [44] and MetaWorld [78]: RoboMimic *Can* and *Square* (each with proficient-human (PH) and multi-human (MH) datasets), RoboMimic *Transport* (MH), and MetaWorld *Stick Push* (stick-push-v3), *Door Open* (door-open-v3), and *Shelf Place* (shelf-place-v3). We use behavioral cloning [55] with an RNN network [29, 22, 26] and behavior cloning with a diffusion action head [14] for the transport and square tasks.<sup>1</sup> For Metaworld tasks, we use SmolVLA [69] (technically, we fine-tune it). The experimental results are summarized in Figure 3 and Figure 5. For all Robomimic tasks considered in

<sup>1</sup>We chose to use BC with an RNN network over the diffusion policy for the can task as the base policy (i.e., the policy with the full dataset) already achieves a 100% success rate, leaving no further room for improvement.

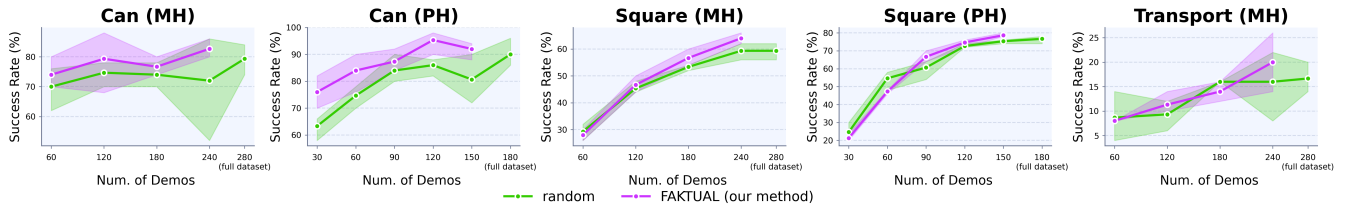


Fig. 3: RoboMimic curation results. Success rates are computed over 50 rollouts for each of the 20 checkpoints, and we report the maximum across checkpoints. Results are averaged over three random seeds, and the error bars indicate the minimum and maximum values. On Can, FAKTUAL consistently outperforms random selection even at the lowest demo counts, and the gap is particularly large for PH, where performance improves sharply with very few demonstrations. For Square, the curves are largely indistinguishable at low demo counts; at higher counts, MH intervals still slightly overlap, while PH shows a small but consistent separation in favor of FAKTUAL. This PH advantage is plausibly due to PH comprising proficient-human, high-quality demonstrations, and to FAKTUAL operating as a diversity-based curation strategy rather than a data-quality-based curation method; (this is in line with the idea of uniform coverage/density discussed in Section I, when the data quality is high). Transport is more challenging: at small budgets FAKTUAL is comparable to or marginally below random pooling, but trends toward an advantage as the demonstration count increases. It is possible that, FAKTUAL will eventually outperform the random pruning strategy as more demonstrations are added and the entropy begins to saturate (see Figure 2).

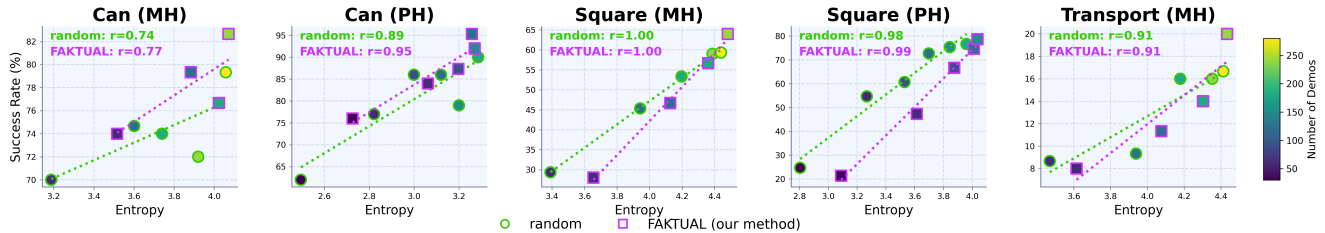


Fig. 4: Signature entropy correlates with success. Success rate versus Signature entropy across RoboMimic tasks (Can, Square, Transport) and dataset variants (MH/PH). Points are different curated subsets colored by the number of demonstrations; dotted lines show linear fits for random selection (green circles) and FAKTUAL (magenta squares). Pearson correlation coefficients ( $r$ ) are reported in each panel, indicating a strong positive association between entropy and downstream success.

this section, we use the corresponding image-based datasets provided by Robomimic.

### B. Real-world Experiments

We evaluate on four real-world manipulation tasks using an SO-ARM101 6-DoF robotic arm kit [73]: *Drawer open*, where the robot opens a closed drawer; *Mug drag*, where it grasps a hook and drags a mug to a goal by using the hook as an intermediate tool; *Pick-and-place marker*, where it grasps a marker and places it into a pen holder; and *Organize objects*, where it follows a simple condition: if a marker is on the table, it places it on a book; otherwise, if a charging brick is on the table, it opens the drawer, places the brick inside, and closes the drawer. We once again use SmolVLA [69] for these real-world tasks. The results are summarized in Figure 6.

### C. Baselines

We compare our method against the following baselines: (1) DemInf [27], a data curation strategy that aims to estimate the relative quality of individual demonstrations in terms of both action diversity and predictability; (2) Cupid [3], a data curation method based on a novel influence function-theoretic formulation for imitation learning policies; (3) DemoSCORE [12], a curation strategy to self-curate based on

online robot experience. More specifically, it trains and cross-validate a classifier to discern successful policy roll-outs from unsuccessful ones and use the classifier to filter demonstrations; (4) Oracle, a method which approximates an upper bound on achievable performance by curating data using privileged access to ground-truth demonstration labels (e.g., indicators of demonstration quality, strategy robustness, or other relevant properties); (5) Success Similarity, a custom baseline from Agia et al. [3] that ranks demonstrations according to average state similarity to successful rollouts; and (6) Random selection. To make fair baseline comparisons fair, we follow the exact experimental setup and implementation from Agia et al. [3]. The results are summarized in Figure 7.<sup>2</sup>

### D. Key observations and discussion

As shown in Figures 3 and 7, in the low-demonstration regime, diversity-maximizing curation can reduce success relative to random selection on harder tasks. This is not universal: on simpler tasks (e.g., Can), promoting diversity does

<sup>2</sup>An important detail is that, in this setting, we use Robomimic’s low-dimensional image representations rather than raw RGB images. Consequently, the reader may therefore observe differences in success rates compared to the previous experiments, and our method does not rely on ViT embeddings here (see Appendix A for more details).

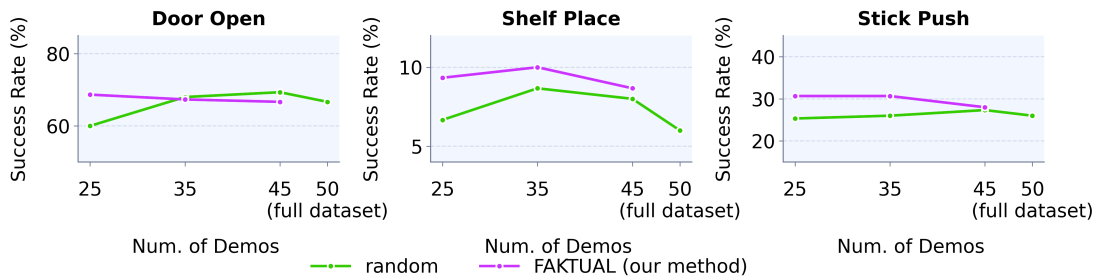


Fig. 5: Metaworld curation results. Success rates are computed over 50 rollouts for each of the 20 checkpoints, and we report the maximum across checkpoints. Metaworld [78] reports substantially different success rates across random seeds; accordingly, we plot only the mean success rate across 3 seeds here, and provide the full per-seed results in Table IV.

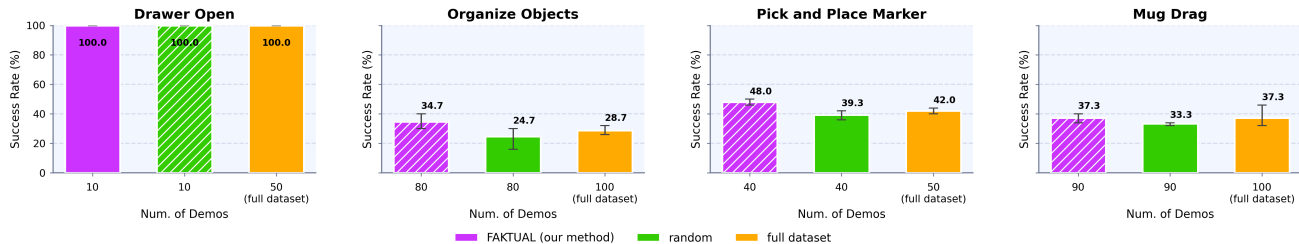


Fig. 6: Real tasks curation results. Success rates are computed over 50 rollouts for each of the 20 checkpoints, and we report the maximum across checkpoints. Results are averaged over three random seeds, and the error bars indicate the minimum and maximum values. Hashed denotes the best-performing method (max success rate); in ties, the simplest method is selected. Two of the three real-world tasks display the curated subset outperforming the full dataset, indicating that additional demonstrations can be redundant and adding noise rather than being strictly beneficial.

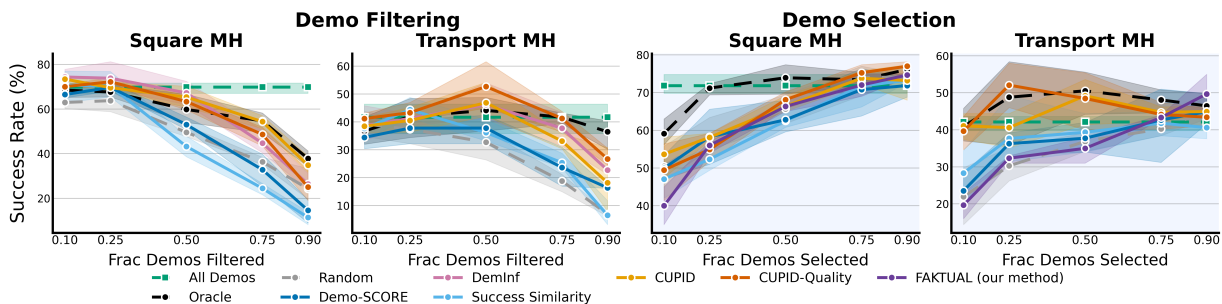


Fig. 7: RoboMimic curation results with baselines. Success rates are computed over 50 rollouts for each of the 20 checkpoints, and we report the maximum across checkpoints. Results are averaged over three random seeds, and the error bars indicate the minimum and maximum values. Relative to random pruning, FAKTUAL is generally better, and it can get you near (and in some spots slightly above) the “All demos” reference—but it’s still below most of the stronger rollout/quality-informed baselines, and it tends to sit closest to DemoSCORE’s performance band. In fact, we expect quality-based curation to outperform diversity-based curation when the dataset includes a mix of high- and low-quality demonstrations (e.g., MH datasets). The key trade is practical: FAKTUAL is model-free and lightweight, so it is a fast “good-enough” curation pass when we cannot afford policy/rollout-dependent scoring or training an auxiliary model.<sup>3</sup>

not noticeably hurt performance. Overall, the demonstration budget at which diversity-aware curation overtakes random selection is task-dependent and typically higher for more difficult tasks. This suggests that discarding redundant or near-duplicate demonstrations becomes beneficial only once the demonstration budget is sufficiently large. This indicates that the intuitive idea of *density* (from Section I) is more important for “harder” tasks, while one can get away with lower density in easier tasks.

We further analyze the effect of diversity on success rate

and Figure 4 shows a strong positive association between signature entropy and downstream success: across tasks, higher-entropy sets consistently achieve higher success rates (Pearson  $r = 0.74\text{--}1.00$  for both random selection and FAKTUAL).

Now we discuss key observations in particular tasks:

a) *Pick-and-place marker*: During data collection for the pick-and-place marker task, the marker position was sampled at the start of each episode from a fixed set of five locations, with a bias toward positions on the left side of the robot. The position of the pen holder was independently sampled from another fixed set of five locations. Applying our method

Method	Auxiliary model?	Modal/Policy-free?	Online rollouts?
CUPID	No	No	Yes
Demo-SCORE	Yes	No	Yes
DemInf	Yes	Yes	No
Success Similarity	No	No	Yes
FAKTUAL	No	Yes	No

TABLE I: Summary of key design characteristics of robot demonstration data curation strategies, categorized by auxiliary model (i.e., an additional learned model beyond the (imitation) policy itself) requirements, dependence on a learned policy, and use of online environment rollouts.

to select demonstrations tends to mitigate this imbalance by approximately equalizing the distribution over marker positions.

*b) Drawer open:* Five distinct lighting conditions were used while collecting demonstrations for the drawer-opening task. Our method did not successfully distinguish between these lighting conditions, primarily because it operates on ViT-based image embeddings or low-dimensional observations (such as point clouds) of the objects of interest, which may not capture global illumination differences sufficiently.

*c) Organize objects:* Because this task is goal-conditioned, our method did not systematically favor trajectories ending in one particular goal configuration over those ending in others.

### VIII. ABLATIONS

*a) Number of signature levels vs. success rate:* We found that the optimal number of signature levels is dependent on the nature of the dataset, and hence on the shape of the trajectories. In Figure 12 (Appendix G) we see two patterns emerge when increasing the number of signature levels: (1) Success rate of the curated dataset improves with size  $m$  (right subplot). (2) Success rate of the curated dataset of size  $m$  improves up to a point, after which it begins to decrease (left subplot).

One possible explanation for this behavior is that, at a very high and intuitive level, the signature transform behaves similarly to a (discrete) Fourier transform: in the Fourier case, the first few coefficients correspond to low frequencies and the higher-order coefficients capture high frequencies, whereas for the signature transform the different levels encode increasingly fine geometric information about the trajectory’s shape. Thus, in datasets where the high-level, coarse shape of the trajectories carries most of the task-relevant information, a truncated signature transform is particularly useful, whereas in settings where this is not the case the full signature becomes important. In some datasets, the detailed shape of the trajectory may not have any meaningful information (e.g., when trajectories are very rough or noisy), in which case the high-level shape is more informative. Throughout this ablation study we use the random Fourier features method over to dynamic programming methods for computing the truncated signature kernel.

*b) Value of  $p$  vs. the Success Rate:* Similar to signature levels, we found that the optimal value for  $p$  is highly dependent on the nature of the dataset. However, choosing a value between 0.2 and 0.5 will result in some improvement over the base policy. In fact, setting  $p = 0$  performs well in practice. This

is because maximizing either the entropy or the determinant maximizes the informal and intuitive notion of diversity.

*c) Signature Kernel vs Global Alignment Kernel:* We benchmarked the signature kernel with the global alignment kernel [17], another effective kernel for sequential data. We found that curating using the global alignment kernel yields the same performance as random selection.

### IX. CONCLUSION AND LIMITATIONS

We introduce signature-based entropy(s) and diversity metrics over demonstrations and used them to develop FAKTUAL, a fast, model-free data curation method for robot imitation learning. Across simulated and real-world benchmarks, diversity-aware curation improved or matched the performance of the full dataset while promoting diversity/entropy ensures the dataset is balanced and follows a more uniform distribution. However, our work has several limitations we discuss below.

**Data quality.** Our method, unlike other data curation strategies such as Chen et al. [12], Hejna et al. [27], Agia et al. [3], does not guarantee the selection of only high-quality trajectories. Future work could combine these approaches

**Datasets used in experiments.** Selecting the most diverse subset can, in some cases, be detrimental, for instance, when a subset of the dataset contains trajectories that are radically different but harmful for learning. None of the datasets used in our experiments contain such adversarial or pathological trajectories, containing only successful demonstrations. In settings where they are present, methods explicitly designed to account for data quality, such as Chen et al. [12], Hejna et al. [27], Agia et al. [3], are likely to be more effective.

**Demo-to-performance relation.** Our approach does not establish strong causal relationships between individual training examples and the resulting policy behavior, a connection that Agia et al. [3] aim to model directly. Hence our method remains susceptible to misattributing the true causes of policy success or failure to the underlying training data.

**Model choice.** We assume the imitation model/policy is good enough to learn from multimodal demonstrations, depending on factors such as the number of parameters, the architecture, the specific task, etc. If the model is not capable of capturing the multimodality in the data, then promoting diversity may actually be harmful; Jia et al. [31]) reports cases where high diversity reduces success when the model is not strong enough. In such cases, random pruning outperforms FAKTUAL.

Despite these limitations, our results highlight trajectory-kernel entropy as a practical tool for measuring and promoting dataset diversity, and motivate a number of directions for future work. For example, extensions on combining diversity- and quality-based curation at larger scales can complement our method to operate in datasets of variable quality.

<sup>3</sup>Note that DemInf can only perform Demo-filtering, while FAKTUAL can only perform Demo-Selection, as trying to perform filtering with FAKTUAL would correspond to finding a set of demos with the lowest diversity and pruning it out, which is ill defined as it would just prune out a "local cluster" of demos.

## REFERENCES

- [1] *The Signature of a Path*, pages 25–40. Springer Berlin Heidelberg, Berlin, Heidelberg, 2007. ISBN 978-3-540-71285-5. doi: 10.1007/978-3-540-71285-5\_2. URL [https://doi.org/10.1007/978-3-540-71285-5\\_2](https://doi.org/10.1007/978-3-540-71285-5_2).
- [2] *Branch and Bound*, chapter 7, pages 113–138. John Wiley & Sons, Ltd, 2020. ISBN 9781119606475. doi: <https://doi.org/10.1002/9781119606475.ch7>. URL <https://onlinelibrary.wiley.com/doi/abs/10.1002/9781119606475.ch7>.
- [3] Christopher Agia, Rohan Sinha, Jingyun Yang, Rika Antonova, Marco Pavone, Haruki Nishimura, Masha Itkina, and Jeannette Bohg. Cupid: Curating data your robot loves with influence functions, 2025. URL <https://arxiv.org/abs/2506.19121>.
- [4] Lucas Barcelos, Tin Lai, Rafael Oliveira, Paulo Borges, and Fabio Ramos. Path signatures for diversity in probabilistic trajectory optimisation. *The International Journal of Robotics Research*, 43(11):1693–1710, 2024. doi: 10.1177/02783649241233300. URL <https://journals.sagepub.com/doi/abs/10.1177/02783649241233300>.
- [5] Suneel Belkhale, Yuchen Cui, and Dorsa Sadigh. Data quality in imitation learning. *Advances in neural information processing systems*, 36:80375–80395, 2023.
- [6] Mostapha Benhenda. ChemGAN challenge for drug discovery: can AI reproduce natural chemical diversity? *arXiv preprint arXiv:1708.08227*, 2017.
- [7] Kevin Black, Noah Brown, Danny Driess, Adnan Esmail, Michael Equi, Chelsea Finn, Niccolo Fusai, Lachy Groom, Karol Hausman, Brian Ichter, et al.  $\pi 0$ : A vision-language-action flow model for general robot control. URL <https://arxiv.org/abs/2410.24164>, 2024.
- [8] Patric Bonnier, Patrick Kidger, Imanol Perez Arribas, Cristopher Salvi, and Terry Lyons. Deep signature transforms, 05 2019.
- [9] Anthony Brohan, Noah Brown, Justice Carbajal, Yevgen Chebotar, Joseph Dabis, Chelsea Finn, Keerthana Gopalakrishnan, Karol Hausman, Alexander Herzog, Jasmine Hsu, Julian Ibarz, Brian Ichter, Alex Irpan, Tomas Jackson, Sally Jesmonth, Nikhil Joshi, Ryan Julian, Dmitry Kalashnikov, Yuheng Kuang, Isabel Leal, Kuang-Huei Lee, Sergey Levine, Yao Lu, Utsav Malla, Deeksha Manjunath, Igor Mordatch, Ofir Nachum, Carolina Parada, Jodilyn Peralta, Emily Perez, Karl Pertsch, Jornell Quiambao, Kanishka Rao, Michael S Ryoo, Grecia Salazar, Pannag R Sanketi, Kevin Sayed, Jaspiar Singh, Sumedh Sontakke, Austin Stone, Clayton Tan, Huong Tran, Vincent Vanhoucke, Steve Vega, Quan H Vuong, Fei Xia, Ted Xiao, Peng Xu, Sichun Xu, Tianhe Yu, and Brianna Zitkovich. RT-1: Robotics Transformer for Real-World Control at Scale. In *Proceedings of Robotics: Science and Systems*, Daegu, Republic of Korea, July 2023. doi: 10.15607/RSS.2023.XIX.025.
- [10] Remi Cadene, Simon Alibert, Alexander Soare, Quentin Gallouedec, Adil Zouitine, Steven Palma, Pepijn Kooijmans, Michel Aractingi, Mustafa Shukor, Dana Aubakirova, Martino Russi, Francesco Capuano, Caroline Pascal, Jade Choghari, Jess Moss, and Thomas Wolf. Lerobot: State-of-the-art machine learning for real-world robotics in pytorch. <https://github.com/huggingface/lerobot>, 2024.
- [11] Annie S Chen, Alec M Lessing, Yuejiang Liu, and Chelsea Finn. Curating demonstrations using online experience. *arXiv preprint arXiv:2503.03707*, 2025.
- [12] Annie S. Chen, Alec M. Lessing, Yuejiang Liu, and Chelsea Finn. Curating demonstrations using online experience, 2025. URL <https://arxiv.org/abs/2503.03707>.
- [13] Ilya Chevyrev and Andrey Kormilitzin. A primer on the signature method in machine learning. 03 2016. doi: 10.48550/arXiv.1603.03788.
- [14] Cheng Chi, Zhenjia Xu, Siyuan Feng, Eric Cousineau, Yilun Du, Benjamin Burchfiel, Russ Tedrake, and Shuran Song. Diffusion policy: Visuomotor policy learning via action diffusion, 2024. URL <https://arxiv.org/abs/2303.04137>.
- [15] Cheng Chi, Zhenjia Xu, Chuer Pan, Eric Cousineau, Benjamin Burchfiel, Siyuan Feng, Russ Tedrake, and Shuran Song. Universal manipulation interface: In-the-wild robot teaching without in-the-wild robots, 2024. URL <https://arxiv.org/abs/2402.10329>.
- [16] Ondřej Cífka, Aliaksei Severyn, Enrique Alfonseca, and Katja Filippova. Eval all, trust a few, do wrong to none: Comparing sentence generation models. *arXiv preprint arXiv:1804.07972*, 2018.
- [17] Marco Cuturi, Jean-Philippe Vert, Oystein Birkenes, and Tomoko Matsui. A kernel for time series based on global alignments. pages II–413, 05 2007. ISBN 1-4244-0728-1. doi: 10.1109/ICASSP.2007.366260.
- [18] Shivin Dass, Alaa Khaddaj, Logan Engstrom, Aleksander Madry, Andrew Ilyas, and Roberto Martín-Martín. Datamil: Selecting data for robot imitation learning with datamodels. *arXiv preprint arXiv:2505.09603*, 2025.
- [19] Adji Bousso Dieng and Amey Pasarkar. A unified and predictive measure of functional diversity. *arXiv preprint arXiv:2509.16133*, 2025.
- [20] Alexey Dosovitskiy, Lucas Beyer, Alexander Kolesnikov, Dirk Weissenborn, Xiaohua Zhai, Thomas Unterthiner, Mostafa Dehghani, Matthias Minderer, Georg Heigold, Sylvain Gelly, Jakob Uszkoreit, and Neil Houlsby. An image is worth 16x16 words: Transformers for image recognition at scale. In *International Conference on Learning Representations*, 2021. URL <https://openreview.net/forum?id=YicbFdNTTy>.
- [21] Anthony Duncan. Von neumann’s 1927 trilogy on the foundations of quantum mechanics. annotated translations, 06 2024.
- [22] Jeffrey L. Elman. Finding structure in time. *Cognitive Science*, 14(2):179–211, 1990. ISSN 0364-0213. doi: [https://doi.org/10.1016/0364-0213\(90\)90002-E](https://doi.org/10.1016/0364-0213(90)90002-E). URL <https://www.sciencedirect.com/science/article/pii/036402139090002E>.

- [23] Dan Friedman and Adji Bousso Dieng. The vendi score: A diversity evaluation metric for machine learning, 2023. URL <https://arxiv.org/abs/2210.02410>.
- [24] Jensen Gao, Annie Xie, Ted Xiao, Chelsea Finn, and Dorsa Sadigh. Efficient data collection for robotic manipulation via compositional generalization, 2024. URL <https://arxiv.org/abs/2403.05110>.
- [25] J. Willard Gibbs. *Elementary Principles in Statistical Mechanics: Developed with Especial Reference to the Rational Foundation of Thermodynamics*. Charles Scribner’s Sons, New York, 1902. URL <https://www.gutenberg.org/ebooks/50992>.
- [26] Ian Goodfellow, Yoshua Bengio, and Aaron Courville. *Deep Learning*. MIT Press, 2016. <http://www.deeplearningbook.org>.
- [27] Joey Hejna, Suvir Mirchandani, Ashwin Balakrishna, Annie Xie, Ayzaan Wahid, Jonathan Tompson, Pannag Sanketi, Dhruv Shah, Coline Devin, and Dorsa Sadigh. Robot data curation with mutual information estimators, 2025. URL <https://arxiv.org/abs/2502.08623>.
- [28] Martin Heusel, Hubert Ramsauer, Thomas Unterthiner, Bernhard Nessler, and Sepp Hochreiter. Gans trained by a two time-scale update rule converge to a local nash equilibrium. *Advances in neural information processing systems*, 30, 2017.
- [29] J J Hopfield. Neural networks and physical systems with emergent collective computational abilities. *Proceedings of the National Academy of Sciences*, 79(8):2554–2558, 1982. doi: 10.1073/pnas.79.8.2554. URL <https://www.pnas.org/doi/abs/10.1073/pnas.79.8.2554>.
- [30] Physical Intelligence, Kevin Black, Noah Brown, James Darpinian, Karan Dhabilia, Danny Driess, Adnan Esmail, Michael Equi, Chelsea Finn, Niccolo Fusai, Manuel Y. Galliker, Dibya Ghosh, Lachy Groom, Karol Hausman, Brian Ichter, Szymon Jakubczak, Tim Jones, Liyiming Ke, Devin LeBlanc, Sergey Levine, Adrian Li-Bell, Mohith Mothukuri, Suraj Nair, Karl Pertsch, Allen Z. Ren, Lucy Xiaoyang Shi, Laura Smith, Jost Tobias Springenberg, Kyle Stachowicz, James Tanner, Quan Vuong, Homer Walke, Anna Walling, Haohuan Wang, Lili Yu, and Ury Zhilinsky.  $\pi_{0.5}$ : a vision-language-action model with open-world generalization, 2025. URL <https://arxiv.org/abs/2504.16054>.
- [31] Xiaogang Jia, Denis Blessing, Xinkai Jiang, Moritz Reuss, Atalay Donat, Rudolf Lioutikov, and Gerhard Neumann. Towards diverse behaviors: A benchmark for imitation learning with human demonstrations, 2024. URL <https://arxiv.org/abs/2402.14606>.
- [32] William Johnson, Joram Lindenstrauss, and Gideon Schechtman. Extensions of lipschitz maps into banach spaces. *Israel Journal of Mathematics*, 54:129–138, 06 1986. doi: 10.1007/BF02764938.
- [33] Jaehun Jung, Seungju Han, Ximing Lu, Skyler Hallinan, David Acuna, Shrimai Prabhunoye, Mostafa Patwary, Mohammad Shoeybi, Bryan Catanzaro, and Yejin Choi. Prismatic synthesis: Gradient-based data diversification boosts generalization in llm reasoning, 2025. URL <https://arxiv.org/abs/2505.20161>.
- [34] Richard M. Karp. *Reducibility among Combinatorial Problems*, pages 85–103. Springer US, Boston, MA, 1972. ISBN 978-1-4684-2001-2. doi: 10.1007/978-1-4684-2001-2\_9. URL [https://doi.org/10.1007/978-1-4684-2001-2\\_9](https://doi.org/10.1007/978-1-4684-2001-2_9).
- [35] Alexander Khazatsky, Karl Pertsch, Suraj Nair, Ashwin Balakrishna, Sudeep Dasari, Siddharth Karamcheti, Soroush Nasiriany, Mohan Kumar Srirama, Lawrence Yunliang Chen, Kirsty Ellis, Peter David Fagan, Joey Hejna, Masha Itkina, Marion Lepert, Yecheng Jason Ma, Patrick Tree Miller, Jimmy Wu, Suneel Belkhale, Shivin Dass, Huy Ha, Arhan Jain, Abraham Lee, Youngwoon Lee, Marius Memmel, Sungjae Park, Ilija Radosavovic, Kaiyuan Wang, Albert Zhan, Kevin Black, Cheng Chi, Kyle Beltran Hatch, Shan Lin, Jingpei Lu, Jean Mercat, Abdul Rehman, Pannag R Sanketi, Archit Sharma, Cody Simpson, Quan Vuong, Homer Rich Walke, Blake Wulfe, Ted Xiao, Jonathan Heewon Yang, Arefeh Yavary, Tony Z. Zhao, Christopher Agia, Rohan Baijal, Mateo Guaman Castro, Daphne Chen, Qiuyu Chen, Trinity Chung, Jaimyn Drake, Ethan Paul Foster, Jensen Gao, David Antonio Herrera, Minh Heo, Kyle Hsu, Jiaheng Hu, Donovan Jackson, Charlotte Le, Yunshuang Li, Roy Lin, Zehan Ma, Abhiram Maddukuri, Suvir Mirchandani, Daniel Morton, Tony Nguyen, Abigail O’Neill, Rosario Scalise, Derick Seale, Victor Son, Stephen Tian, Emi Tran, Andrew E. Wang, Yilin Wu, Annie Xie, Jingyun Yang, Patrick Yin, Yunchu Zhang, Osbert Bastani, Glen Berseth, Jeannette Bohg, Ken Goldberg, Abhinav Gupta, Abhishek Gupta, Dinesh Jayaraman, Joseph J Lim, Jitendra Malik, Roberto Martín-Martín, Subramanian Ramamoorthy, Dorsa Sadigh, Shuran Song, Jiajun Wu, Michael C. Yip, Yuke Zhu, Thomas Kollar, Sergey Levine, and Chelsea Finn. DROID: A Large-Scale In-The-Wild Robot Manipulation Dataset. In *Proceedings of Robotics: Science and Systems*, Delft, Netherlands, July 2024. doi: 10.15607/RSS.2024.XX.120.
- [36] Samir Khuller, Anna Moss, and Joseph (Seffi) Naor. The budgeted maximum coverage problem. *Information Processing Letters*, 70(1):39–45, 1999. ISSN 0020-0190. doi: [https://doi.org/10.1016/S0020-0190\(99\)00031-9](https://doi.org/10.1016/S0020-0190(99)00031-9). URL <https://www.sciencedirect.com/science/article/pii/S0020019099000319>.
- [37] Moo Jin Kim, Karl Pertsch, Siddharth Karamcheti, Ted Xiao, Ashwin Balakrishna, Suraj Nair, Rafael Rafailov, Ethan P Foster, Pannag R Sanketi, Quan Vuong, Thomas Kollar, Benjamin Burchfiel, Russ Tedrake, Dorsa Sadigh, Sergey Levine, Percy Liang, and Chelsea Finn. Openvla: An open-source vision-language-action model. In Pulkit Agrawal, Oliver Kroemer, and Wolfram Burgard, editors, *Proceedings of The 8th Conference on Robot Learning*, volume 270 of *Proceedings of Machine Learning Research*, pages 2679–2713. PMLR, 06–09 Nov 2025.
- [38] Franz J. Kiraly and Harald Oberhauser. Kernels for sequentially ordered data. *Journal of Machine Learning*

- Research*, 20(31):1–45, 2019. URL <http://jmlr.org/papers/v20/16-314.html>.
- [39] Tamara G. Kolda and Brett W. Bader. Tensor decompositions and applications. *SIAM Review*, 51(3): 455–500, 2009. doi: 10.1137/07070111X. URL <https://doi.org/10.1137/07070111X>.
- [40] Sachit Kuhar, Shuo Cheng, Shivang Chopra, Matthew Bronars, and Danfei Xu. Learning to discern: Imitating heterogeneous human demonstrations with preference and representation learning. In Jie Tan, Marc Toussaint, and Kourosh Darvish, editors, *Proceedings of The 7th Conference on Robot Learning*, volume 229 of *Proceedings of Machine Learning Research*, pages 1437–1449. PMLR, 06–09 Nov 2023.
- [41] Alex Kulesza. Determinantal point processes for machine learning. *Foundations and Trends® in Machine Learning*, 5(2–3):123–286, 2012. ISSN 1935-8245. doi: 10.1561/22000000044. URL <http://dx.doi.org/10.1561/22000000044>.
- [42] Darrick Lee and Harald Oberhauser. The signature kernel, 2023. URL <https://arxiv.org/abs/2305.04625>.
- [43] Terry Lyons. Rough paths, signatures and the modelling of functions on streams. 05 2014.
- [44] Ajay Mandlekar, Danfei Xu, Josiah Wong, Soroush Nasiriany, Chen Wang, Rohun Kulkarni, Li Fei-Fei, Silvio Savarese, Yuke Zhu, and Roberto Martín-Martín. What matters in learning from offline human demonstrations for robot manipulation, 2021. URL <https://arxiv.org/abs/2108.03298>.
- [45] Reginald McLean, Evangelos Chatzaroulas, Luc McCutcheon, Frank Röder, Tianhe Yu, Zhanpeng He, K.R. Zentner, Ryan Julian, J K Terry, Isaac Woungang, Nariman Farsad, and Pablo Samuel Castro. Meta-world+: An improved, standardized, RL benchmark. In *The Thirty-ninth Annual Conference on Neural Information Processing Systems Datasets and Benchmarks Track*, 2025. URL <https://openreview.net/forum?id=1de3azE606>.
- [46] Baharan Mirzasoleiman, Ashwinkumar Badanidiyuru, Amin Karbasi, Jan Vondrak, and Andreas Krause. Lazier than lazy greedy, 2014. URL <https://arxiv.org/abs/1409.7938>.
- [47] Muhammad Ferjad Naeem, Seong Joon Oh, Youngjung Uh, Yunjey Choi, and Jaejun Yoo. Reliable fidelity and diversity metrics for generative models. In *International Conference on Machine Learning*, pages 7176–7185. PMLR, 2020.
- [48] G. L. Nemhauser, L. A. Wolsey, and M. L. Fisher. An analysis of approximations for maximizing submodular set functions–i. *Math. Program.*, 14(1):265–294, December 1978. ISSN 0025-5610. doi: 10.1007/BF01588971. URL <https://doi.org/10.1007/BF01588971>.
- [49] J. von Neumann. Thermodynamik quantenmechanischer gesamtheiten. *Nachrichten von der Gesellschaft der Wissenschaften zu Göttingen, Mathematisch-Physikalische Klasse*, 1927:273–291, 1927. URL <http://eudml.org/doc/59231>.
- [50] Quan Nguyen and Adji Bousso Dieng. Vendi information gain: An alternative to mutual information for science and machine learning, 2025. URL <https://arxiv.org/abs/2505.09007>.
- [51] Octo Model Team, Dibya Ghosh, Homer Walke, Karl Pertsch, Kevin Black, Oier Mees, Sudeep Dasari, Joey Hejna, Charles Xu, Jianlan Luo, Tobias Kreiman, You Liang Tan, Lawrence Yunliang Chen, Pannag Sanketi, Quan Vuong, Ted Xiao, Dorsa Sadigh, Chelsea Finn, and Sergey Levine. Octo: An open-source generalist robot policy. In *Proceedings of Robotics: Science and Systems*, Delft, Netherlands, 2024.
- [52] Motoya Ohnishi, Ireteiyao Akinola, Jie Xu, Ajay Mandlekar, and Fabio Ramos. Signatures meet dynamic programming: Generalizing Bellman equations for trajectory following. In Alessandro Abate, Mark Cannon, Kostas Margellos, and Antonis Papachristodoulou, editors, *Proceedings of the 6th Annual Learning for Dynamics & Control Conference*, volume 242 of *Proceedings of Machine Learning Research*, pages 466–479. PMLR, 15–17 Jul 2024. URL <https://proceedings.mlr.press/v242/ohnishi24a.html>.
- [53] Abby O’Neill, Abdul Rehman, Abhiram Maddukuri, Abhishek Gupta, Abhishek Padalkar, Abraham Lee, Acorn Pooley, Agrim Gupta, Ajay Mandlekar, Ajinkya Jain, Albert Tung, Alex Bewley, Alex Herzog, Alex Irpan, Alexander Khazatsky, Anant Rai, Anchit Gupta, Andrew Wang, Anikait Singh, Animesh Garg, Aniruddha Kembhavi, Annie Xie, Anthony Brohan, Antonin Raffin, Archit Sharma, Arefeh Yavary, Arhan Jain, Ashwin Balakrishna, Ayzaan Wahid, Ben Burgess-Limerick, Beomjoon Kim, Bernhard Schölkopf, Blake Wulfe, Brian Ichter, Cewu Lu, Charles Xu, Charlotte Le, Chelsea Finn, Chen Wang, Chenfeng Xu, Cheng Chi, Chenguang Huang, Christine Chan, Christopher Agia, Chuer Pan, Chuyuan Fu, Coline Devin, Danfei Xu, Daniel Morton, Danny Driess, Daphne Chen, Deepak Pathak, Dhruv Shah, Dieter Büchler, Dinesh Jayaraman, Dmitry Kalashnikov, Dorsa Sadigh, Edward Johns, Ethan Foster, Fangchen Liu, Federico Ceola, Fei Xia, Feiyu Zhao, Freek Stulp, Gaoyue Zhou, Gaurav S. Sukhatme, Gautam Salhotra, Ge Yan, Gilbert Feng, Giulio Schiavi, Glen Berseth, Gregory Kahn, Guanzhi Wang, Hao Su, Hao-Shu Fang, Haochen Shi, Henghui Bao, Heni Ben Amor, Henrik I Christensen, Hiroki Furuta, Homer Walke, Hongjie Fang, Huy Ha, Igor Mordatch, Ilija Radosavovic, Isabel Leal, Jacky Liang, Jad Abou-Chakra, Jaehyung Kim, Jaimyn Drake, Jan Peters, Jan Schneider, Jasmine Hsu, Jeannette Bohg, Jeffrey Bingham, Jeffrey Wu, Jensen Gao, Jiaheng Hu, Jiayuan Wu, Jialin Wu, Jiankai Sun, Jianlan Luo, Jiayuan Gu, Jie Tan, Jihoon Oh, Jimmy Wu, Jingpei Lu, Jingyun Yang, Jitendra Malik, João Silvério, Joey Hejna, Jonathan Booher, Jonathan Tompson, Jonathan Yang, Jordi Salvador, Joseph J. Lim, Junhyek Han, Kaiyuan Wang, Kanishka Rao, Karl Pertsch, Karol Hausman, Keegan Go, Keerthana Gopalakrishnan, Ken Goldberg, Kendra Byrne, Kenneth Oslund, Kento Kawaharazuka, Kevin

- Black, Kevin Lin, Kevin Zhang, Kiana Ehsani, Kiran Lekkala, Kirsty Ellis, Krishan Rana, Krishnan Srinivasan, Kuan Fang, Kunal Pratap Singh, Kuo-Hao Zeng, Kyle Hatch, Kyle Hsu, Laurent Itti, Lawrence Yunliang Chen, Lerrel Pinto, Li Fei-Fei, Liam Tan, Linxi Jim Fan, Lionel Ott, Lisa Lee, Luca Weihs, Magnum Chen, Marion Lepert, Marius Memmel, Masayoshi Tomizuka, Masha Itkina, Mateo Guaman Castro, Max Spero, Maximilian Du, Michael Ahn, Michael C. Yip, Mingtong Zhang, Mingyu Ding, Minh Heo, Mohan Kumar Srirama, Mohit Sharma, Moo Jin Kim, Naoaki Kanazawa, Nicklas Hansen, Nicolas Heess, Nikhil J Joshi, Niko Suenderhauf, Ning Liu, Norman Di Palo, Nur Muhammad Mahi Shafiullah, Oier Mees, Oliver Kroemer, Osbert Bastani, Pannag R Sanketi, Patrick Tree Miller, Patrick Yin, Paul Wohlhart, Peng Xu, Peter David Fagan, Peter Mitrano, Pierre Sermanet, Pieter Abbeel, Priya Sundareshan, Qiuyu Chen, Quan Vuong, Rafael Rafailov, Ran Tian, Ria Doshi, Roberto Martín-Martín, Rohan Bajjal, Rosario Scalise, Rose Hendrix, Roy Lin, Runjia Qian, Ruohan Zhang, Russell Mendonca, Rutav Shah, Ryan Hoque, Ryan Julian, Samuel Bustamante, Sean Kirmani, Sergey Levine, Shan Lin, Sherry Moore, Shikhar Bahl, Shivin Dass, Shubham Sonawani, Shuran Song, Sichun Xu, Siddhant Haldar, Siddharth Karamcheti, Simeon Adebola, Simon Guist, Soroush Nasiriany, Stefan Schaal, Stefan Welker, Stephen Tian, Subramanian Ramamoorthy, Sudeep Dasari, Suneel Belkhale, Sungjae Park, Suraj Nair, Suvir Mirchandani, Takayuki Osa, Tanmay Gupta, Tatsuya Harada, Tatsuya Matsushima, Ted Xiao, Thomas Kollar, Tianhe Yu, Tianli Ding, Todor Davchev, Tony Z. Zhao, Travis Armstrong, Trevor Darrell, Trinity Chung, Vidhi Jain, Vincent Vanhoucke, Wei Zhan, Wenxuan Zhou, Wolfram Burgard, Xi Chen, Xiaolong Wang, Xinghao Zhu, Xinyang Geng, Xiyuan Liu, Xu Liangwei, Xuanlin Li, Yao Lu, Yecheng Jason Ma, Yejin Kim, Yevgen Chebotar, Yifan Zhou, Yifeng Zhu, Yilin Wu, Ying Xu, Yixuan Wang, Yonatan Bisk, Yoonyoung Cho, Youngwoon Lee, Yuchen Cui, Yue Cao, Yueh-Hua Wu, Yujin Tang, Yuke Zhu, Yunchu Zhang, Yunfan Jiang, Yunshuang Li, Yunzhu Li, Yusuke Iwasawa, Yutaka Matsuo, Zehan Ma, Zhuo Xu, Zichen Jeff Cui, Zichen Zhang, and Zipeng Lin. Open x-embodiment: Robotic learning datasets and rt-x models : Open x-embodiment collaboration0. In *2024 IEEE International Conference on Robotics and Automation (ICRA)*, pages 6892–6903, 2024. doi: 10.1109/ICRA57147.2024.10611477.
- [54] Sagar Parekh, Heramb Nemlekar, and Dylan P. Losey. Towards balanced behavior cloning from imbalanced datasets, 2026. URL <https://arxiv.org/abs/2508.06319>.
- [55] Dean A. Pomerleau. Alvin: An autonomous land vehicle in a neural network. In D. Touretzky, editor, *Advances in Neural Information Processing Systems*, volume 1. Morgan-Kaufmann, 1988. URL [https://proceedings.neurips.cc/paper\\_files/paper/1988/file/812b4ba287f5ee0bc9d43bbf5bbe87fb-Paper.pdf](https://proceedings.neurips.cc/paper_files/paper/1988/file/812b4ba287f5ee0bc9d43bbf5bbe87fb-Paper.pdf).
- [56] Jose Gallego Posada, Ankit Vani, Max Schwarzer, and Simon Lacoste-Julien. Gait: A geometric approach to information theory. In *International Conference on Artificial Intelligence and Statistics*, pages 2601–2611. PMLR, 2020.
- [57] Kristina Preuer, Philipp Renz, Thomas Unterthiner, Sepp Hochreiter, and Günter Klambauer. Fréchet ChemNet distance: a metric for generative models for molecules in drug discovery. *Journal of chemical information and modeling*, 58(9):1736–1741, 2018.
- [58] Mohammad Reza Rezaei and Adji Bousso Dieng. Vendirag: Adaptively trading-off diversity and quality significantly improves retrieval augmented generation with llms. *arXiv preprint arXiv:2502.11228*, 2025.
- [59] Olivier Roy and Martin Vetterli. The effective rank: A measure of effective dimensionality. In *2007 15th European Signal Processing Conference*, pages 606–610, 2007.
- [60] Walter Rudin. *Principles of Mathematical Analysis*. McGraw-Hill, New York, 3 edition, 1976. ISBN 007054235X.
- [61] Mehdi SM Sajjadi, Olivier Bachem, Mario Lucic, Olivier Bousquet, and Sylvain Gelly. Assessing generative models via precision and recall. In *Proceedings of the 32nd International Conference on Neural Information Processing Systems*, pages 5234–5243, 2018.
- [62] Tim Salimans, Ian Goodfellow, Wojciech Zaremba, Vicki Cheung, Alec Radford, Xi Chen, and Xi Chen. Improved Techniques for Training GANs. In D. D. Lee, M. Sugiyama, U. V. Luxburg, I. Guyon, and R. Garnett, editors, *Advances in Neural Information Processing Systems 29*, pages 2234–2242. Curran Associates, Inc., 2016.
- [63] Christopher Salvi, Thomas Cass, James Foster, Terry Lyons, and Weixin Yang. The signature kernel is the solution of a goursat pde. *SIAM Journal on Mathematics of Data Science*, 3(3):873–899, 2021. doi: 10.1137/20M1366794. URL <https://doi.org/10.1137/20M1366794>.
- [64] Kanthi K. Sarpatwar, Baruch Schieber, and Hadas Shachnai. Constrained submodular maximization via greedy local search. *Operations Research Letters*, 47(1): 1–6, 2019. ISSN 0167-6377. doi: <https://doi.org/10.1016/j.orl.2018.11.002>. URL <https://www.sciencedirect.com/science/article/pii/S0167637718300038>.
- [65] Anna Scampicchio and Melanie N. Zeilinger. On the role of the signature transform in nonlinear systems and data-driven control, 2025. URL <https://arxiv.org/abs/2409.05685>.
- [66] C. E. Shannon. A mathematical theory of communication. *The Bell System Technical Journal*, 27(3):379–423, 1948. doi: 10.1002/j.1538-7305.1948.tb01338.x.
- [67] Tianxiao Shen, Myle Ott, Michael Auli, and Marc’Aurelio Ranzato. Mixture models for diverse machine translation: Tricks of the trade. In *International conference on machine learning*, pages 5719–5728. PMLR, 2019.
- [68] Modi Shi, Li Chen, Jin Chen, Yuxiang Lu, Chiming

- Liu, Guanghui Ren, Ping Luo, Di Huang, Maoqing Yao, and Hongyang Li. Is diversity all you need for scalable robotic manipulation?, 2025. URL <https://arxiv.org/abs/2507.06219>.
- [69] Mustafa Shukor, Dana Aubakirova, Francesco Capuano, Pepijn Kooijmans, Steven Palma, Adil Zouitine, Michel Aractingi, Caroline Pascal, Martino Russi, Andres Marafioti, Simon Alibert, Matthieu Cord, Thomas Wolf, and Remi Cadene. Smolvla: A vision-language-action model for affordable and efficient robotics, 2025. URL <https://arxiv.org/abs/2506.01844>.
- [70] Sreevardhan Sirigiri, Christian Hughes, Ian Abraham, and Fabio Ramos. Diversifying parallel ergodic search: A signature kernel evolution strategy. In *The Thirty-ninth Annual Conference on Neural Information Processing Systems*, 2025. URL <https://openreview.net/forum?id=3XuUnUEI7e>.
- [71] A. Srivastava, L. Valkov, C. Russell, M. U. Gutmann, and C. Sutton. VEEGAN: reducing mode collapse in GANs using implicit variational learning. In *Advances in Neural Information Processing Systems*, 2017.
- [72] Christian Szegedy, Vincent Vanhoucke, Sergey Ioffe, Jon Shlens, and Zbigniew Wojna. Rethinking the Inception architecture for computer vision. In *Proceedings of the IEEE conference on computer vision and pattern recognition*, pages 2818–2826, 2016.
- [73] TheRobotStudio and Hugging Face. Standard Open SO-100 & SO-101 Arms. <https://github.com/TheRobotStudio/SO-ARM100>. Accessed: 2025-11-19.
- [74] Csaba Tóth, Harald Oberhauser, and Zoltán Szabó. Random fourier signature features. *SIAM Journal on Mathematics of Data Science*, 7(1):329–354, 2025. doi: 10.1137/23M1620478. URL <https://doi.org/10.1137/23M1620478>.
- [75] David P. Williamson and David B. Shmoys. *The Design of Approximation Algorithms*. Cambridge University Press, USA, 1st edition, 2011. ISBN 0521195276.
- [76] L.A. Wolsey and G.L. Nemhauser. *Integer and Combinatorial Optimization*. Wiley Series in Discrete Mathematics and Optimization. Wiley, 1999. ISBN 9780471359432. URL <https://books.google.com/books?id=vvm4DwAAQBAJ>.
- [77] Weixin Yang, Terry Lyons, Hao Ni, Cordelia Schmid, and Lianwen Jin. *Developing the Path Signature Methodology and Its Application to Landmark-Based Human Action Recognition*, pages 431–464. Springer International Publishing, Cham, 2022. ISBN 978-3-030-98519-6. doi: 10.1007/978-3-030-98519-6\_18. URL [https://doi.org/10.1007/978-3-030-98519-6\\_18](https://doi.org/10.1007/978-3-030-98519-6_18).
- [78] Tianhe Yu, Deirdre Quillen, Zhanpeng He, Ryan Julian, Avnish Narayan, Hayden Shively, Adithya Bellathur, Karol Hausman, Chelsea Finn, and Sergey Levine. Meta-world: A benchmark and evaluation for multi-task and meta reinforcement learning, 2021. URL <https://arxiv.org/abs/1910.10897>.
- [79] Yu Yu, Shahram Khadivi, and Jia Xu. Can data diversity enhance learning generalization? In Nicoletta Calzolari, Chu-Ren Huang, Hansaem Kim, James Pustejovsky, Leo Wanner, Key-Sun Choi, Pum-Mo Ryu, Hsin-Hsi Chen, Lucia Donatelli, Heng Ji, Sadao Kurohashi, Patrizia Paggio, Nianwen Xue, Seokhwan Kim, Younggyun Hahm, Zhong He, Tony Kyungil Lee, Enrico Santus, Francis Bond, and Seung-Hoon Na, editors, *Proceedings of the 29th International Conference on Computational Linguistics*, pages 4933–4945, Gyeongju, Republic of Korea, October 2022. International Committee on Computational Linguistics. URL <https://aclanthology.org/2022.coling-1.437/>.
- [80] Xuyu Zhang, Haofan Huang, Dawei Zhang, Songlin Zhuang, Shensheng Han, Puxiang Lai, and Honglin Liu. Cross-dataset generalization in deep learning, 2024. URL <https://arxiv.org/abs/2410.11207>.
- [81] Yu Zhang, Yuqi Xie, Huihan Liu, Rutav Shah, Michael Wan, Linxi Fan, and Yuke Zhu. Scizor: A self-supervised approach to data curation for large-scale imitation learning, 2025. URL <https://arxiv.org/abs/2505.22626>.
- [82] Brianna Zitkovich, Tianhe Yu, Sichun Xu, Peng Xu, Ted Xiao, Fei Xia, Jialin Wu, Paul Wohlhart, Stefan Welker, Ayzaan Wahid, Quan Vuong, Vincent Vanhoucke, Huong Tran, Radu Soricut, Anikait Singh, Jaspiar Singh, Pierre Sermanet, Pannag R. Sanketi, Grecia Salazar, Michael S. Ryoo, Krista Reymann, Kanishka Rao, Karl Pertsch, Igor Mordatch, Henryk Michalewski, Yao Lu, Sergey Levine, Lisa Lee, Tsang-Wei Edward Lee, Isabel Leal, Yuheng Kuang, Dmitry Kalashnikov, Ryan Julian, Nikhil J. Joshi, Alex Irpan, Brian Ichter, Jasmine Hsu, Alexander Herzog, Karol Hausman, Keerthana Gopalakrishnan, Chuyuan Fu, Pete Florence, Chelsea Finn, Kumar Avinava Dubey, Danny Driess, Tianli Ding, Krzysztof Marcin Choromanski, Xi Chen, Yevgen Chebotar, Justice Carbajal, Noah Brown, Anthony Brohan, Montserrat Gonzalez Arenas, and Kehang Han. Rt-2: Vision-language-action models transfer web knowledge to robotic control. In Jie Tan, Marc Toussaint, and Kourosh Darvish, editors, *Proceedings of The 7th Conference on Robot Learning*, volume 229 of *Proceedings of Machine Learning Research*, pages 2165–2183. PMLR, 06–09 Nov 2023. URL <https://proceedings.mlr.press/v229/zitkovich23a.html>.

## APPENDIX CONTENTS

<b>A</b>	<b>Demos to Paths</b>	14
<b>B</b>	<b>Signature Kernel</b>	15
<b>C</b>	<b>Approximating the Truncated Signature Kernel with Random Fourier features</b>	16
<b>D</b>	<b>Background on Submodularity</b>	18
<b>E</b>	<b>Algorithms for computing the maximum <math>m</math>-subset</b>	18
<b>F</b>	<b>Implementation Details</b>	19

<b>G</b>	<b>Additional Results</b>	22
<b>H</b>	<b>Related Works Covering Dataset Diversity in General ML</b>	24
<b>I</b>	<b>Proofs</b>	25

APPENDIX A  
DEMOS TO PATHS

For simplicity, we assume a single camera and a single robot; however, our method extends straightforwardly to settings with multiple cameras and robots.

*A. Method 1: Flatten and Stacked*

A demonstration  $d_i \in \mathcal{D}$  typically consists of various modalities such as states, actions, the robot’s perception data (e.g., RGB images from cameras, depth sensor measurements, etc.), rewards, and any additional auxiliary data recorded at each time step  $t \in T_i$ , where  $T_i$  denotes the length of the demonstration. We denote the state at time  $t$  in  $d_i$  by  $s_i(t)$ , the action by  $a_i(t)$ , the RGB image by  $I_i^{\text{RGB}}(t)$ , and the reward by  $R_i(t)$ .

To convert a demonstration into a trajectory (or path), at each time step  $t \in T_i$  we first embed the RGB image into a fixed dimensional ViT [20] embedding  $e_i(t)$ . Alternatively, one can also extract low-dimensional representation (such as point clouds, ground truth pose(s) etc.) of the objects of interest from the RGB images, we will denote this with  $l_i(t)$  (if  $l_i(t)$  is not vector, one can simply flatten it into a vector).<sup>4</sup> Let  $o_i(t) := e_i(t)$  or  $l_i(t)$  denote the "observation" vector at time  $t \in T_i$ . We then construct a feature vector by flattening and concatenating all components:

$$X_i(t) = \begin{bmatrix} s_i(t) \\ a_i(t) \\ o_i(t) \\ \vdots \\ R_i(t) \end{bmatrix}.$$

Now one can use the signature kernel over the trajectories  $X_i$ .

*B. Method 2: Convex Combination*

The reader may observe that each data type (or modality) (e.g., states ( $s_i(t)$ ), actions ( $a_i(t)$ ), observations ( $o_i(t)$ ), and rewards) forms a path or trajectory in its own right. Consequently, for each such path we can compute a signature kernel, and then take a convex combination of these kernels. Mathematically, let

$$k_{\text{state}}^{\text{sig}}, k_{\text{action}}^{\text{sig}}, k_{\text{observations}}^{\text{sig}}, \dots, k_{\text{reward}}^{\text{sig}}$$

denote the signature kernels corresponding to the state, action, observations, reward trajectories, etc.. We then define the

<sup>4</sup>All experiments in Section VII used the ViT embedding method except the results presented in Figure 7. We provide a limited evaluation of the robomimic’s lift task using the low-dimensional representation in Appendix G.

combined kernel as

$$\hat{k}^{\text{sig}} = \alpha_{\text{state}} k_{\text{state}}^{\text{sig}} + \alpha_{\text{action}} k_{\text{action}}^{\text{sig}} + \alpha_{\text{observations}} k_{\text{observations}}^{\text{sig}} + \dots + \alpha_{\text{reward}} k_{\text{reward}}^{\text{sig}},$$

where the coefficients satisfy

$$\alpha_{\text{state}}, \alpha_{\text{action}}, \alpha_{\text{observations}}, \dots, \alpha_{\text{reward}} \geq 0, \quad \text{and} \\ \alpha_{\text{state}} + \alpha_{\text{action}} + \alpha_{\text{observations}} + \dots + \alpha_{\text{reward}} = 1.$$

This convex combination allows us to integrate information from multiple modalities in a principled way, while preserving the kernel’s validity.<sup>5</sup> Furthermore,  $\hat{k}^{\text{sig}}$  will inherit many useful properties of the signature kernel (e.g. universality).

*C. Method 3: Low dim convex combination*

Alternatively, one can use a simpler convex combination using the signature kernel and the RBF kernel defined as

$$k^{\text{RBF}}(x, x') = \exp\left(-\frac{\|x - x'\|^2}{2h^2}\right). \quad (9)$$

We use the first frame from each observation video, denoted  $I_i^{\text{RGB}}(0)$ , and compute either a ViT embedding or a low-dimensional observation from  $I_i^{\text{RGB}}(0)$ . Let  $p_i(t)$  denote the end-effector path of demonstration  $d_i$  at time  $t$ . Using these quantities, we can construct a kernel matrix as follows:

$$\hat{K}^{\text{mix}} = \alpha_1 K^{\text{RBF}} + \alpha_2 K^{\text{sig}}, \quad \sum \alpha_i = 1$$

where  $K_{i,j}^{\text{RBF}} = k^{\text{rbf}}(o_i(0), o_j(0))$  and  $K_{i,j}^{\text{sig}} = k^{\text{sig}}(p_i(t), p_j(t))$ .

*D. Implementational practices*

*a) Time coordinate:* It is important to note that, in practice, it can sometimes be useful to append a monotonic “time” coordinate to each path (e.g.,  $s'_i(t) := (t, s_i(t))$ ). This adjustment is necessary because the signature transform is reparameterization invariant.

For example, consider the following constant paths:

$$p_1(t) = \delta_a, \quad p_2(t) = \delta_b, \quad 0 \leq t \leq 1, \quad a, b \in [0, 1], \quad a \neq b,$$

for which we obtain

$$\varphi(p_1) = \varphi(p_2).$$

However, after augmenting with time, we have

$$p'_1(t) = (t, \delta_a), \quad p'_2(t) = (t, \delta_b), \\ 0 \leq t \leq 1, \quad a, b \in [0, 1], \quad a \neq b,$$

and in this case

$$\varphi(p'_1) \neq \varphi(p'_2).$$

This modification can sometimes be detrimental, and its impact is highly task- and dataset-dependent; in scenarios where reparameterization invariance is important, we do not recommend appending the time coordinate.

<sup>5</sup>Although in our experiments this method did not yield better outcomes than the previous approach, it may scale more effectively with higher-dimensional settings (e.g., longer horizons) and additionally allows for individual kernel hyperparameter control for each modality.

b) *Sub-sampling*: It is not always necessary to use the states, actions, and observations, etc. at all time steps  $t \in T$ ; for long-horizon tasks, it can be beneficial to sample them at regular intervals, especially to reduce the overall computational load.

c) *Distractors*: It is important to note that when using the method described in Subsection A-C or applying sub-sampling, distractors may not be captured adequately. This issue will particularly be pronounced when a distractor appears and disappears within a time interval shorter than the sampling period under sub-sampling, or when it only appears later in the trajectory while the method in Subsection A-C relies on earlier observations.

d) *Camera selection*: If the dataset includes wrist-mounted cameras, we recommend not using them with the methods described above, as they can introduce substantial noise and make all demonstrations look diverse. In fact, we strongly advise using only a single camera that reliably captures the entire scene.

## APPENDIX B SIGNATURE KERNEL

### A. Signature Transform

**Definition 7. Signature transform of a path (trajectory) [63].** Let  $V$  be a Banach space and consider the tensor algebra of formal power series

$$T((V)) := \prod_{k \geq 0} V^{\otimes k},$$

equipped with the natural operations induced by the tensor product and with unit element  $(1, 0, 0, \dots)$ .

Let  $x : I \rightarrow V$  be a continuous path on a compact interval  $I \subset \mathbb{R}$  with finite  $p$ -variation for some  $p < 2$ . For any subinterval  $[s, t] \subset I$ , the signature of  $x$  over  $[s, t]$  is the element of  $T((V))$  defined by the sequence of iterated integrals

$$\varphi(x)_{s,t} = \left( 1, \int_{s < u_1 < t} dx(u_1), \dots, \int_{s < u_1 < \dots < u_k < t} dx(u_1) \otimes \dots \otimes dx(u_k), \dots \right). \quad (10)$$

The signature provides a feature representation of the path and is invariant to reparameterization, i.e.,  $\varphi(x) = \varphi(x \circ \theta)$  for any increasing reparameterization  $\theta$ .

#### 1) Properties of the Signature Transform:

a) *Injectivity*: The path signature can be viewed as a canonical feature map that embeds a multivariate path into an (infinite) sequence of iterated integrals. It is injective on the class of non-tree-like paths: two such paths cannot share the same full signature. In practice, non-tree-likeness is typically enforced by augmenting the path with a monotone ‘‘time’’ coordinate.

b) *Time-reversal duality*: The signature also satisfies a time-reversal duality relation:

$$\varphi(x)_{a,b} \otimes \varphi(\overleftarrow{x})_{a,b} = 1,$$

where 1 denotes the unit element and  $\overleftarrow{x}(t) := x(a + b - t)$ .

c) *Chen’s identity*: A central property of signatures is their multiplicative behavior under concatenation. If a path is decomposed into successive segments, then the signature of the entire path can be obtained by tensor-multiplying the signatures of the segments. This is formalized by Chen’s identity.

**Theorem 1 (Chen’s identity).** Consider the same setting as Definition 7, then for any  $a \leq s \leq u \leq t \leq b$ ,

$$\varphi(x)_{s,t} = \varphi(x)_{s,u} \otimes \varphi(x)_{u,t} \in T((V)).$$

Alternatively, for each level  $k \geq 0$ ,

$$\varphi(x)_{s,t}^k = \sum_{i+j=k} \varphi(x)_{s,u}^i \otimes \varphi(x)_{u,t}^j,$$

where  $\varphi(x)_{a,b}^\ell \in V^{\otimes \ell}$  is the  $\ell$ -th iterated integral.

In Hopf-algebraic terms,  $\varphi(x)$  is *group-like* in the tensor algebra, i.e., its coproduct satisfies

$$\Delta \varphi(x) = \varphi(x) \otimes \varphi(x).$$

d) *Factorial decay of signature terms*: For a path  $x$  of finite  $p$ -variation with  $p > 1$ , the norms of the level- $k$  iterated integrals exhibit factorial decay [43]:

$$\left\| \int_{s < u_1 < \dots < u_k < t} dx(u_1) \otimes \dots \otimes dx(u_k) \right\|_{V^{\otimes k}} \leq \frac{\|x\|_{p,[s,t]}^k}{k!},$$

where  $\|x\|_{p,[s,t]}$  denotes the  $p$ -variation of  $x$  over  $[s, t]$ . Consequently, the signature (and signature kernel) can often be well-approximated by truncation at a finite level  $L \in \mathbb{N}$ . The truncated signature of level  $L$  is

$$\varphi^L(x)_{s,t} = \left( 1, \int_{s < u_1 < t} dx(u_1), \dots, \int_{s < u_1 < \dots < u_L < t} dx(u_1) \otimes \dots \otimes dx(u_L) \right) \in \bigoplus_{k=0}^L V^{\otimes k}, \quad (11)$$

where  $\bigoplus$  denotes the direct sum.

### B. Signature Kernel

We now introduce the signature kernel, which uses the signature transform as a feature map to define a positive-definite kernel on paths.

**Definition 8. Signature kernel.** Consider the same setting as Definition 8, then the signature kernel  $k^{\text{sig}}(x, y) : I \times J \rightarrow \mathbb{R}$  is defined as

$$k_{s,t}^{\text{sig}}(x, y) = \langle \varphi(x)_{u,s}, \varphi(y)_{v,t} \rangle, \quad (12)$$

where  $\varphi(x)_{u,s}$  and  $\varphi(y)_{v,t}$  denote the signatures of  $x$  and  $y$  over the subintervals  $[u, s]$  and  $[v, t]$ , respectively, and  $\langle \cdot, \cdot \rangle$  denotes the canonical inner product on the (truncated or completed) tensor algebra.

Computing the untruncated signature kernel: Leveraging the kernel trick of [63], the (untruncated) signature kernel can be evaluated efficiently by solving a simple PDE.

**Theorem 2.** Let  $I = [u, u']$  and  $J = [v, v']$  be compact intervals, and let  $x \in \mathcal{C}^1(I, V)$  and  $y \in \mathcal{C}^1(J, V)$ . Then the signature kernel  $k^{\text{sig}}(x, y)$  satisfies the linear second-order hyperbolic partial differential equation

$$\frac{\partial^2}{\partial s \partial t} k_{s,t}^{\text{sig}}(x, y) = \langle \dot{x}(s), \dot{y}(t) \rangle_V k_{s,t}^{\text{sig}}(x, y),$$

with boundary conditions

$$k_{u,t}^{\text{sig}}(x, y) = 1 \quad \forall t \in J, \quad k_{s,v}^{\text{sig}}(x, y) = 1 \quad \forall s \in I.$$

This PDE characterization of the signature kernel enables efficient evaluation using standard numerical schemes, including finite-difference and finite-element discretizations, as well as other appropriate schemes.

Computing the full  $(n \times n)$  Gram matrix for  $n$  trajectories/paths of length  $T$  in  $\mathbb{R}^d$  via dynamic programming has time complexity  $O(n^2 T^2 d^c)$ , where  $c$  depends on the truncation level of the signature transform. Using the kernel trick in Theorem 2, the kernel between two paths can be evaluated in as little as  $O(T^2 d)$ . Forming the entire Gram matrix still requires  $n^2$  pairwise evaluations, and thus the overall cost remains  $O(n^2 T^2 d)$ . However, the underlying PDE formulation is amenable to efficient parallelization. In particular, an explicit finite-difference implementation on a sufficiently provisioned GPU can reduce the per-pair computation to effectively linear scaling in the trajectory length in practice, yielding an effective wall-clock complexity of  $O(T d)$  assuming the GPU can support the required level of parallelism [63].

## APPENDIX C

### APPROXIMATING THE TRUNCATED SIGNATURE KERNEL WITH RANDOM FOURIER FEATURES

Computing the signature kernel exactly requires working in an infinite-dimensional RKHS, which becomes intractable for long or high-dimensional sequences. To overcome this, we approximate the truncated signature transform via Random Fourier Features (RFF), yielding finite-dimensional feature maps whose inner products concentrate uniformly to the true signature kernel with high probability.

#### A. Background on Random Fourier Features

Random Fourier Features provide a practical way to approximate any continuous, bounded, shift-invariant kernel  $k(x, y) = k(x - y)$  on  $\mathbb{R}^d$ . By Bochner's theorem, there exists a probability measure  $\Lambda$  on  $\mathbb{R}^d$  (the spectral measure of  $k$ ) such that

$$k(x - y) = \int_{\mathbb{R}^d} e^{i w^\top (x - y)} d\Lambda(w).$$

Drawing  $d$ -dimensional frequencies  $w_1, \dots, w_{\tilde{d}} \stackrel{iid}{\sim} \Lambda$ , we define the RFF map

$$\tilde{\varphi}(x) = \frac{1}{\sqrt{\tilde{d}}} [\cos(w_1^\top x), \sin(w_1^\top x), \dots, \cos(w_{\tilde{d}}^\top x), \sin(w_{\tilde{d}}^\top x)]^\top \in \mathbb{R}^{2\tilde{d}}.$$

This satisfies

$$\mathbb{E}[\langle \tilde{\varphi}(x), \tilde{\varphi}(y) \rangle] = k(x, y),$$

so the empirical kernel  $\tilde{k}(x, y) = \langle \tilde{\varphi}(x), \tilde{\varphi}(y) \rangle$  gives an unbiased approximation with error decaying exponentially in  $\tilde{d}$  under mild moment conditions on  $\Lambda$ .

#### B. Random Fourier Signature Features

To approximate the  $L$ -truncated signature kernel

$$k_{\text{Sig}}^{\leq L}(x, y) = \langle \varphi_{\text{Sig}}^{\leq L}(x), \varphi_{\text{Sig}}^{\leq L}(y) \rangle,$$

in a finite-dimensional space, we replace each inner-product evaluation of the base kernel on path increments by an unbiased Random Fourier Features (RFF) estimator. Specifically, drawing

$$W^{(1)}, \dots, W^{(L)} \stackrel{iid}{\sim} \Lambda^{\tilde{d}},$$

from the spectral measure  $\Lambda$  of a shift-invariant kernel on  $\mathbb{R}^d$ , we obtain RFF maps

$$\tilde{\varphi}_m(x) = \frac{1}{\sqrt{\tilde{d}}} (\cos(W^{(m)\top} x), \sin(W^{(m)\top} x)) \in \mathbb{R}^{2\tilde{d}},$$

which satisfy

$$\mathbb{E}[\langle \tilde{\varphi}_m(x), \tilde{\varphi}_m(y) \rangle] = k(x, y).$$

By replacing each kernel evaluation  $k(x_{i_p+1} - x_{i_p}, y_{j_p+1} - y_{j_p})$  in the tensor-product expansion of the signature kernel with the inner product  $\langle \tilde{\varphi}_p(x_{i_p+1}) - \tilde{\varphi}_p(x_{i_p}), \tilde{\varphi}_p(y_{j_p+1}) - \tilde{\varphi}_p(y_{j_p}) \rangle$ , we obtain a feature map  $\tilde{\varphi}_{\text{Sig}}^{\leq L}(x)$  of total dimension  $\sum_{m=0}^L (2\tilde{d})^m$ , whose evaluation for a sequence  $x \in X_{\text{seq}}$  of length  $\ell_x$  can be computed in

$$O(L \tilde{d} \ell_x)$$

time. Moreover, the resulting approximate kernel

$$\tilde{k}_{\text{Sig}}^{\leq L}(x, y) = \langle \tilde{\varphi}_{\text{Sig}}^{\leq L}(x), \tilde{\varphi}_{\text{Sig}}^{\leq L}(y) \rangle$$

is unbiased, i.e.  $\mathbb{E}[\tilde{k}_{\text{Sig}}^{\leq L}(x, y)] = k_{\text{Sig}}^{\leq L}(x, y)$ , and concentrates uniformly to the true signature kernel as  $\tilde{d} \rightarrow \infty$  under standard moment conditions on  $\Lambda$ .

**Definition 9** (Random Fourier Signature Features). Let  $W^{(1)}, \dots, W^{(L)} \stackrel{iid}{\sim} \Lambda^{\tilde{d}}$  be i.i.d. RFF weight matrices for RFF dimension  $\tilde{d}$ , and define for each  $m \in [L]$  the RFF map

$$\tilde{\varphi}_m(x) = \frac{1}{\sqrt{\tilde{d}}} (\cos(W^{(m)\top} x), \sin(W^{(m)\top} x)) \in \mathbb{R}^{2\tilde{d}}.$$

For a sequence  $x = (x_1, \dots, x_{\ell_x}) \in X_{\text{seq}}$ , the  $L$ -truncated RFSF map is

$$\tilde{\varphi}_{\text{Sig}}^{\leq L}(x) = (\tilde{\varphi}_{\text{Sig}}^m(x))_{m=0}^L, \quad \tilde{\varphi}_{\text{Sig}}^0(x) = 1,$$

$$\tilde{\varphi}_{\text{Sig}}^m(x) = \sum_{i \in \Delta_m(\ell_x-1)} (\tilde{\varphi}_1(x_{i_1+1}) - \tilde{\varphi}_1(x_{i_1})) \otimes \cdots \otimes (\tilde{\varphi}_m(x_{i_m+1}) - \tilde{\varphi}_m(x_{i_m})), \quad m \geq 1,$$

where  $\Delta_m(n) = \{1 \leq i_1 < \cdots < i_m \leq n\}$ . Its associated kernel is

$$\begin{aligned} \tilde{k}_{\text{Sig}}^{\leq L}(x, y) &= \langle \tilde{\varphi}_{\text{Sig}}^{\leq L}(x), \tilde{\varphi}_{\text{Sig}}^{\leq L}(y) \rangle \\ &= \sum_{m=0}^L \sum_{i \in \Delta_m(\ell_x-1)} \sum_{j \in \Delta_m(\ell_y-1)} \prod_{p=1}^m \delta_{i_p, j_p}^2 \langle \tilde{\varphi}_p(x_{i_{p+1}}) - \tilde{\varphi}_p(x_{i_p}), \\ &\quad \tilde{\varphi}_p(y_{j_{p+1}}) - \tilde{\varphi}_p(y_{j_p}) \rangle. \end{aligned} \quad (13)$$

To ensure exponential-type concentration in the RFF dimension  $\tilde{d}$ , we impose the standard Bernstein-moment condition on the spectral measure  $\Lambda$ :

$$\mathbb{E}_{w \sim \Lambda} [|w_i|^{2k}] \leq k! S^2 R^{k-2}, \quad \forall k \geq 2, \quad (14)$$

for constants  $S, R > 0$ .

Under this condition, the RFSF kernel is not only unbiased (by construction) but satisfies the following uniform approximation guarantee:

**Theorem 3** (Uniform approximation of the signature kernel). *Let  $k_{\text{Sig}}^m$  be the  $m$ -th level component of the true signature kernel and  $\tilde{k}_{\text{Sig}}^m$  the corresponding RFSF level- $m$  approximation. Under (14), for any compact  $X \subset \mathbb{R}^d$ , 1-variation bound  $V$ , and  $m \leq L$ , it holds for all  $\epsilon > 0$  that*

$$\mathbb{P} \left[ \sup_{\substack{x, y \in X_{\text{seq}} \\ \|x\|_{1\text{-var}}, \|y\|_{1\text{-var}} \leq V}} |k_{\text{Sig}}^m(x, y) - \tilde{k}_{\text{Sig}}^m(x, y)| \geq \epsilon \right] \leq \begin{cases} (C_{d,X} (\frac{\beta_{d,m,V}}{\epsilon})^{d/(d+1)} + d) \exp(-\frac{\tilde{d}}{2(d+1)(S^2+R)} (\frac{\epsilon}{\beta_{d,m,V}})^2), & \epsilon < \beta_{d,m,V}, \\ (C_{d,X} (\frac{\beta_{d,m,V}}{\epsilon})^{d/((d+1)m)} + d) \exp(-\frac{\tilde{d}}{2(d+1)(S^2+R)} (\frac{\epsilon}{\beta_{d,m,V}})^{1/m}), & \epsilon \geq \beta_{d,m,V}, \end{cases} \quad (15)$$

where  $C_{d,X}, \beta_{d,m,V} > 0$  depend on  $X, V, d, m, S, R$ .

### C. Dimensionality reduction: Diagonal projection

Although the RFSF map  $\tilde{\varphi}_{\text{Sig}}^{\leq L}(x)$  lives in a finite-dimensional space, its  $m$ -th level tensor has  $(2\tilde{d})^m$  entries, which quickly becomes prohibitive. To alleviate this, we observe that the level- $m$  RFSF kernel can be written as

$$\tilde{k}_{\text{Sig}}^m(x, y) = \frac{1}{\tilde{d}^m} \sum_{q_1, \dots, q_m=1}^{\tilde{d}} \sum_{i \in \Delta_m(\ell_x-1)} \sum_{j \in \Delta_m(\ell_y-1)} \prod_{p=1}^m \delta_{i_p, j_p}^2 \cos(w_{q_p}^{(p)\top} (x_{i_p} - y_{j_p})), \quad (16)$$

by expanding each RFF kernel in Definition 9 and  $\delta^2$  denotes a 2<sup>nd</sup>-order cross-differencing operator such that  $\delta_{i,j}^2 k(x_i, y_j) := k(x_{i+1}, y_{j+1}) + k(x_i, y_j) - k(x_{x+1}, y_j) - k(x_i, y_{j+1})$ . We then restrict the outer sum over the Cartesian product  $[\tilde{d}]^m$  to its

diagonal multi-indices  $\{(q, \dots, q) : q = 1, \dots, \tilde{d}\}$ , yielding a dramatically smaller feature set.

**Definition 10** (Diagonally Projected RFSF). *Let  $w_1^{(m)}, \dots, w_{\tilde{d}}^{(m)}$  i.i.d.  $\sim \Lambda$  for each  $m = 1, \dots, L$ . For  $q = 1, \dots, \tilde{d}$  and  $m \geq 1$  define*

$$\hat{\varphi}_{m,q}(x) = (\cos(w_q^{(m)\top} x), \sin(w_q^{(m)\top} x)) \in \mathbb{R}^2.$$

The  $L$ -truncated diagonally projected RFSF map is

$$\hat{\varphi}_{\text{Sig}}^{\leq L}(x) = (\hat{\varphi}_{\text{Sig}}^m(x))_{m=0}^L, \quad \hat{\varphi}_{\text{Sig}}^0(x) = 1,$$

$$\hat{\varphi}_{\text{Sig}}^m(x) = \frac{1}{\sqrt{\tilde{d}}} \left( \sum_{i \in \Delta_m(\ell_x-1)} \delta \hat{\varphi}_{1,q}(x_{i_1}) \otimes \cdots \otimes \delta \hat{\varphi}_{m,q}(x_{i_m}) \right)_{q=1}^{\tilde{d}}.$$

The associated kernel is

$$\tilde{k}_{\text{Sig}}^{\text{DP}, \leq L}(x, y) = \sum_{m=0}^L \frac{1}{\tilde{d}} \sum_{q=1}^{\tilde{d}} \sum_{i \in \Delta_m(\ell_x-1)} \sum_{j \in \Delta_m(\ell_y-1)} \prod_{p=1}^m \delta_{i_p, j_p}^2 \hat{k}_{m,q}(x_{i_p}, y_{j_p}), \quad (17)$$

where  $\hat{k}_{m,q}(u, v) = \langle \hat{\varphi}_{m,q}(u), \hat{\varphi}_{m,q}(v) \rangle$ . Note that  $\dim \bigoplus_{m=0}^L (\mathbb{R}^2)^{\otimes m} = \sum_{m=0}^L 2^m = 2^{L+1} - 1$ , so the overall feature dimension is  $\tilde{d}(2^{L+1} - 1)$ .

The following result shows that this drastic reduction still yields a high-quality approximation:

**Theorem 4** (Concentration for the RFSF-DP kernel). *Under the Bernstein moment condition  $\mathbb{E}[|w_i|^{2k}] \leq k! S^2 R^{k-2}$ , for each level  $m \leq L$  and error  $\epsilon > 0$ ,*

$$\mathbb{P} [ |\tilde{k}_{\text{Sig}}^m(x, y) - \tilde{k}_{\text{Sig}}^{\text{DP}, m}(x, y)| \geq \epsilon ] \leq 2 \exp\left(-\frac{1}{4} \min\left\{ \frac{\tilde{d} \epsilon^2}{4 C_{d,m,x,y}^2}, \left(\frac{\tilde{d} \epsilon}{\sqrt{8} C_{d,m,x,y}}\right)^{1/m} \right\}\right), \quad (18)$$

where

$$\begin{aligned} C_{d,m,x,y} &\leq \sqrt{8e^4(2\pi)^{1/4}e^{1/24}} (4e^3 \|x\|_{1\text{-var}} \|y\|_{1\text{-var}} / m)^{m/2} \\ &\quad \times \sqrt{(2d \max(S, R))^m + \left(\frac{L^2}{\ln 2}\right)^m}. \end{aligned}$$

In practice, forming  $\hat{\varphi}_{\text{Sig}}^{\leq L}(x)$  for  $N$  sequences of length  $\ell$  costs

$$O(N \ell \tilde{d} (Ld + 2L)),$$

i.e. *linear* in both sequence length  $\ell$  and RFF sample size  $\tilde{d}$ .

### D. Dimensionality reduction: Tensor Random Projection

Random projections provide a way to reduce the dimensionality of high-order tensors while approximately preserving inner products, via the Johnson–Lindenstrauss lemma [32]. In the tensor setting, one uses CP (CANDECOMP/PARAFAC [39]) rank-1 random projections, which act on an  $m$ -th order tensor  $s \in (\mathbb{R}^{2\tilde{d}})^{\otimes m}$  by

$$\text{Pr}(s) = \langle p^{(1)} \otimes \cdots \otimes p^{(m)}, s \rangle,$$

where each  $p^{(r)} \sim \mathcal{N}(0, I_{2\tilde{d}})$  is i.i.d. Gaussian. Stacking  $\tilde{d}$  independent such functionals yields a map TRP :  $(\mathbb{R}^{2\tilde{d}})^{\otimes m} \rightarrow \mathbb{R}^{\tilde{d}}$  with only  $O(m\tilde{d})$  parameters instead of  $O((2\tilde{d})^m)$ .

**Definition 11** (Tensor Random Projected RFSF). Let  $W^{(1)}, \dots, W^{(L)}$  i.i.d.  $\Lambda^{\tilde{d}}$  be as in Definition 9, and let

$$P^{(m)} = (p_1^{(m)}, \dots, p_{\tilde{d}}^{(m)}) \in \mathbb{R}^{2\tilde{d} \times \tilde{d}}, \quad p_q^{(m)} \stackrel{iid}{\sim} \mathcal{N}(0, I_{2\tilde{d}}),$$

for  $m = 1, \dots, L$ . Define the  $L$ -truncated RFSF-TRP map

$$\check{\varphi}_{\text{Sig}}^{\leq L}(x) = \frac{1}{\sqrt{\tilde{d}}} (\check{\varphi}_{\text{Sig}}^m(x))_{m=0}^L, \quad \check{\varphi}_{\text{Sig}}^0(x) = 1,$$

where for  $m \geq 1$ ,

$$\check{\varphi}_{\text{Sig}}^m(x) = \sum_{i \in \Delta_m(\ell_x - 1)} (P^{(1)\top} \delta \check{\varphi}_1(x_{i_1})) \odot \dots \odot (P^{(m)\top} \delta \check{\varphi}_m(x_{i_m})) \in \mathbb{R}^{\tilde{d}}, \quad (19)$$

with  $\delta \check{\varphi}_m(x_t) = \check{\varphi}_m(x_{t+1}) - \check{\varphi}_m(x_t)$  and  $\odot$  the Hadamard product. The corresponding RFSF-TRP kernel is

$$\begin{aligned} \tilde{k}_{\text{Sig}}^{\text{TRP}, \leq L}(x, y) &= \left\langle \check{\varphi}_{\text{Sig}}^{\leq L}(x), \check{\varphi}_{\text{Sig}}^{\leq L}(y) \right\rangle \\ &= \sum_{m=0}^L \frac{1}{\tilde{d}} \sum_{q=1}^{\tilde{d}} \sum_{i \in \Delta_m(\ell_x - 1)} \sum_{j \in \Delta_m(\ell_y - 1)} \\ &\quad \times \prod_{p=1}^m \langle p_q^{(p)}, \delta \check{\varphi}_p(x_{i_p}) \rangle \langle p_q^{(p)}, \delta \check{\varphi}_p(y_{j_p}) \rangle. \end{aligned} \quad (20)$$

By construction  $\tilde{k}_{\text{Sig}}^{\text{TRP}, \leq L}(x, y)$  is an unbiased estimator of the true signature kernel, and under the Bernstein-moment condition (14) it concentrates subexponentially in  $\tilde{d}$ :

**Theorem 5** (Concentration for the RFSF-TRP kernel). For each  $m \leq L$  and any  $\epsilon > 0$ , there exists an absolute constant  $C_{d, \Lambda} = 2 \left(1 + \frac{S^2}{2R} + \frac{S^2}{4R^2}\right)^{\tilde{d}}$  such that

$$\mathbb{P} \left[ \left| \tilde{k}_{\text{Sig}}^m(x, y) - \tilde{k}_{\text{Sig}}^{\text{TRP}, m}(x, y) \right| \geq \epsilon \right] \leq C_{d, \Lambda} \exp \left( - \left( \frac{m^2 \tilde{d}^{1/(2m)} \epsilon^{1/m}}{2\sqrt{2}e^3 R \|x\|_{1\text{-var}} \|y\|_{1\text{-var}}} \right)^{1/2} \right),$$

where  $\tilde{k}_{\text{Sig}}^{\text{TRP}, m}$  is the level- $m$  component of (20).

Finally, computing  $\check{\varphi}_{\text{Sig}}^{\leq L}(x)$  for  $N$  sequences of length  $\ell$  costs

$$O(N \ell \tilde{d} (L \tilde{d} + \tilde{d})),$$

i.e. linear in the sequence length and RF dimension except for a mild quadratic term in  $\tilde{d}$ .

In practice, the RFSF-DP and RFSF-TRP variants provide excellent trade-offs between feature dimensionality and approximation quality, allowing signature-kernel methods to scale to large datasets with theoretical guarantees.

## APPENDIX D

### BACKGROUND ON SUBMODULARITY

In this section, we aim to provide a background on submodular functions.

**Definition 12** (Subset Function). Given a ground set  $\mathcal{U}$ , a subset function is a function

$$f : 2^{\mathcal{U}} \rightarrow \mathbb{R},$$

that maps each subset of  $\mathcal{U}$  to a real value.

**Definition 13** (Monotone Non-decreasing Function). A (subset) function is monotone non-decreasing if

$$\forall A \subseteq B \subseteq \mathcal{U} : f(A) \leq f(B).$$

**Definition 14** (Submodular Function). A (subset) function  $f : 2^{\mathcal{U}} \rightarrow \mathbb{R}$  is submodular if

$$f(A+x) - f(A) \geq f(B+x) - f(B), \quad \forall A \subseteq B \subseteq \mathcal{U}, x \in \mathcal{U} \setminus B.$$

## APPENDIX E

### ALGORITHMS FOR COMPUTING THE MAXIMUM $m$ -SUBSET

Using the same notation as in Sections V and VI, the maximum coverage problem in our setting can be formulated as the following integer program:

$$\begin{aligned} &\text{maximize} && f(D) \\ &\text{subject to} && D \subseteq \mathcal{D}, \\ &&& |D| = m \text{ and } m \leq |\mathcal{D}| \end{aligned}$$

where consider  $f(\cdot) = S(\cdot)$  or  $f(\cdot) = \Delta(\cdot)$ .

In practice, it is often convenient to use the regularized objective

$$\begin{aligned} \Delta'(D) &:= \log \det(K^{\text{sig}} + \mu I_{m \times m}), \\ K_{i,j}^{\text{sig}} &= k^{\text{sig}}(d_i, d_j), \quad d_i, d_j \in D, \quad \mu \in \mathbb{R}_{>0}, \end{aligned}$$

instead of  $\Delta$ . This modification does not change the solution of the optimization problem. However, it is advantageous in two respects:  $\Delta'$  is more numerically stable, and  $\Delta'$  is submodular (see Definition 14).

In general, integer programming problems are NP-hard. Consequently, computing an exact solution is feasible only for very small datasets. In such cases, one may employ branch-and-bound methods to solve the problem exactly [76, 2]. For larger instances, integer programs can often be approximated in polynomial time using various algorithmic techniques (see, e.g., [75]). In this work, we focus on a set of simple and easy-to-implement algorithms.

### A. Greedy Local Search

Given the ground set  $\mathcal{D}$  and a objective  $f : 2^{\mathcal{V}} \rightarrow \mathbb{R}$  and cardinality bound  $m$ , we first greedily build a size- $m$  set  $X$  by repeatedly adding the element with maximum marginal gain. Then we optionally apply local search: while there exists a single-element swap that improves  $f$ , we perform it.

a) *Approximation guarantee*: For a nonnegative, monotone, submodular function  $f$  under a simple cardinality constraint  $|X| \leq m$ , the classical greedy algorithm [48, 64] achieves a  $(1 - 1/e)$ -approximation, and any subsequent local search that only performs improving moves preserves this guarantee. If  $f$  is non-submodular this algorithm provides no guarantee, however in practice this will perform fairly well.

---

**Algorithm 1** Greedy Local Search (cardinality  $m$ )

---

```
1: Input: ground set  $\mathcal{D}$ , objective  $f(\cdot)$ , integer  $m$ 
2:  $X \leftarrow \emptyset$  ▷ greedy initialization
3: for  $i = 1$  to  $m$  do
4:   choose  $e \in \mathcal{D} \setminus X$  maximizing  $G(e | X) = f(X \cup \{e\}) - f(X)$ 
5:   if  $G(e | X) \leq 0$  then
6:     break
7:   end if
8:    $X \leftarrow X \cup \{e\}$ 
9: end for ▷ 1-swap local search
10: while there exist  $e \in X, e' \in \mathcal{D} \setminus X$  s.t.  $f(X \setminus \{e\} \cup \{e'\}) > f(X)$  do
11:    $X \leftarrow X \setminus \{e\} \cup \{e'\}$ 
12: end while
13: return  $X$ 
```

---

### B. Stochastic Greedy

Given a ground set  $\mathcal{D}$  of size  $n$ , a objective function  $f$  and a cardinality constraint  $m$ , the stochastic greedy algorithm maintains a solution set  $X$ . At each of  $m$  iterations it samples a random subset of the remaining elements of size  $\lceil (n/m) \log(1/\varepsilon) \rceil$ , evaluates marginal gains only on this sample, and adds the sampled element with the largest marginal gain.

---

**Algorithm 2** Stochastic Greedy (cardinality  $m$ )

---

```
1: Input: ground set  $\mathcal{D}$ , objective  $f(\cdot)$ , integers  $n = |\mathcal{D}|$ ,  $m$ , parameter  $\varepsilon \in (0, 1)$ 
2:  $X \leftarrow \emptyset$ 
3:  $X_{\text{val}} \leftarrow f(X)$ 
4:  $r \leftarrow \lceil (n/m) \log(1/\varepsilon) \rceil$ 
5: for  $i = 1$  to  $m$  do
6:    $A \leftarrow \mathcal{D} \setminus X$  ▷ remaining elements
7:   if  $A = \emptyset$  then
8:     break
9:   end if
10:  sample  $R \subseteq A$  uniformly without replacement with  $|R| = \min\{|A|, r\}$ 
11:   $e^* \leftarrow \arg \max_{e \in R} (f(X \cup \{e\}) - X_{\text{val}})$ 
12:   $X \leftarrow X \cup \{e^*\}$ 
13:   $X_{\text{val}} \leftarrow f(X)$ 
14: end for
15: return  $X$ 
```

---

a) *Approximation guarantee.*: Let  $f$  be nonnegative, monotone, and submodular. For any  $\varepsilon \in (0, 1)$ , the stochastic greedy algorithm above, with  $r = \lceil (n/m) \log(1/\varepsilon) \rceil$ , returns a random set  $X$  such that  $\mathbb{E}[f(X)] \geq (1 - 1/e - \varepsilon) f(X^*)$ , where  $X^*$  is an optimal solution of size at most  $m$  [46]. The expected number of function evaluations is  $O(n \log(1/\varepsilon))$ , independent of  $m$ .

### C. Sampling an $m$ -DPP on $\mathcal{D}$ .

Another principled way to select a diverse subset of elements from the ground set  $\mathcal{D}$  is via determinantal point processes (DPPs) [41].<sup>6</sup> In an L-ensemble DPP with kernel  $L \propto K^{\text{sig}} + \mu I$ , the probability of a subset  $X \subseteq \mathcal{D}$  is proportional to  $\det(L_{X,X})$ , so that maximizing  $\Delta(X)$  (or  $\Delta'(X)$ ) is exactly the maximum a posteriori (MAP) inference problem for this DPP. We next describe the corresponding DPP-based algorithm for selecting a diverse subset of size  $m$ .

Let  $\mathcal{D} = \{d_1, \dots, d_N\}$  be the ground set and  $\tilde{K}^{\text{sig}} \in \mathbb{R}^{N \times N}$  the full similarity matrix,

$$\tilde{K}_{i,j}^{\text{sig}} = k^{\text{sig}}(d_i, d_j), \quad d_i, d_j \in \mathcal{D}.$$

We define the L-ensemble kernel

$$L := \tilde{K}^{\text{sig}} + \mu I_{N \times N}, \quad \mu \in \mathbb{R}_{>0},$$

so that for any subset  $X \subseteq \mathcal{D}$  with  $|X| = m$ ,  $\Delta'(X) = \log \det(L_{X,X})$  is (up to an additive constant) the log-probability under the corresponding  $m$ -DPP. The following algorithm samples a random subset  $X$  of size  $m$  from this  $m$ -DPP.

## APPENDIX F

### IMPLEMENTATION DETAILS

#### A. Robomimic Tasks

For all Robomimic's tasks we use the official implementation provided by Robomimic [44]. We now provide a brief description of the tasks, however we recommend the interested reader to consult [44] for the complete details.

##### 1) Task Description:

- **Can.** The robot must move a coke can from a large bin into a smaller target bin. This task is slightly more challenging than Lift, as grasping the can is more difficult than grasping the cube, and the robot must also accurately place the can into the bin. At the start of each episode, the can's pose is randomized within the left bin, with its z-rotation sampled randomly.
- **Square.** The robot must pick up a square nut and place it onto a rod. This task is substantially more difficult than Lift and Pick Place Can because it requires precise manipulation to both grasp the nut and insert it onto the rod. At the start of each episode, the square nut's pose is randomized within a square region on the table, including a randomly sampled z-rotation.
- **Transport.** Two robot arms must collaboratively transfer a hammer from a closed container on one shelf to a target bin on another shelf. One arm is responsible for retrieving the hammer from the container, while the other clears the target bin by moving a piece of trash into a nearby receptacle. Finally, one arm passes the hammer to the other, which then places it in the target bin. At the start of each episode, the positions of all bins, the lid, the trash

<sup>6</sup>We choose only provide a very brief introduction, DPPs in general require a lot of mathematical machinery and background that is beyond the scope of this article, hence we strongly recommend the interested reader to consult [41].

---

**Algorithm 3** Sampling an  $m$ -DPP on  $\mathcal{D}$ 

---

**Require:** Ground set  $\mathcal{D} = \{d_1, \dots, d_N\}$ , similarity kernel  $k^{\text{sig}}$ , regularizer  $\mu > 0$ , target size  $m$ .

1: Form  $\tilde{K}^{\text{sig}} \in \mathbb{R}^{N \times N}$  with  $\tilde{K}_{ij}^{\text{sig}} = k^{\text{sig}}(d_i, d_j)$ , and set  $L \leftarrow \tilde{K}^{\text{sig}} + \mu I_{N \times N}$ .

2: Compute eigendecomposition  $L = \sum_{n=1}^N \lambda_n v_n v_n^\top$ , with eigenvalues  $\lambda_n \geq 0$  and orthonormal eigenvectors  $v_n \in \mathbb{R}^N$ .

**Phase 1: choose  $m$  eigenvectors.**

3: Initialize elementary symmetric polynomials  $e_n^\ell$  for  $n = 0, \dots, N$ ,  $\ell = 0, \dots, m$ :

$$e_0^0 \leftarrow 1, \quad e_n^0 \leftarrow 1 \text{ for } n = 1, \dots, N, \\ e_0^\ell \leftarrow 0 \text{ for } \ell = 1, \dots, m.$$

4: **for**  $\ell = 1, \dots, m$  **do**

5:   **for**  $n = 1, \dots, N$  **do**

6:      $e_n^\ell \leftarrow e_{n-1}^{\ell-1} + \lambda_n e_{n-1}^{\ell-1}$

7:   **end for**

8: **end for**

9:  $J \leftarrow \emptyset$ ,  $\ell \leftarrow m$ .

10: **for**  $n = N, N-1, \dots, 1$  **do**

11:   **if**  $\ell = 0$  **then**

12:     **break**

13:   **end if**

14:   Draw  $u \sim \text{Uniform}[0, 1]$ .

15:   **if**  $u \leq \lambda_n e_{n-1}^{\ell-1} / e_n^\ell$  **then**

16:      $J \leftarrow J \cup \{n\}$ ,  $\ell \leftarrow \ell - 1$ .

17:   **end if**

18: **end for**

19: Let  $V \leftarrow \{v_n : n \in J\}$  be the selected eigenvectors.

**Phase 2: sample items given  $V$ .**

20:  $Y \leftarrow \emptyset$ .      $\triangleright Y \subseteq \{1, \dots, N\}$  will index items in  $\mathcal{D}$

21: **while**  $V \neq \emptyset$  **do**

22:   For each  $i \in \{1, \dots, N\}$ , set

$$\Pr(i) \propto \sum_{v \in V} (v_i)^2$$

and sample  $i$  according to  $\Pr(i)$ .

23:    $Y \leftarrow Y \cup \{i\}$ .

24:   Update  $V$  to an orthonormal basis for the subspace of  $\text{span}(V)$  orthogonal to the standard basis vector  $e_i$ .

25: **end while**

26: **return**  $X = \{d_i : i \in Y\} \subseteq \mathcal{D}$  with  $|X| = m$ .

---

cube, and the hammer are randomized within small square regions. Additionally, the z-rotations of the trash cube and the hammer are randomized over ranges of 108 and 60 degrees, respectively.

2) *Dataset Description:* The PH datasets contain 200 demonstrations collected by a single, experienced teleoperator, whereas the MH datasets contain 300 demonstrations collected by 6 teleoperators of varying proficiency, each contributing



(a) Can Task      (b) Square Task      (c) Transport Task

Fig. 8: Scene visualization of the 3 Robomimic tasks.

50 demonstrations. The 6 teleoperators are partitioned into a “better” group of 2 experienced operators, an “okay” group of 2 adequately skilled operators, and a “worse” group of 2 inexperienced operators.

In our experiments in Figure 3, we used 20 demonstrations for validation and 180 for training when using the PH datasets, and 30 demonstrations for validation and 270 for training when using the MH datasets.

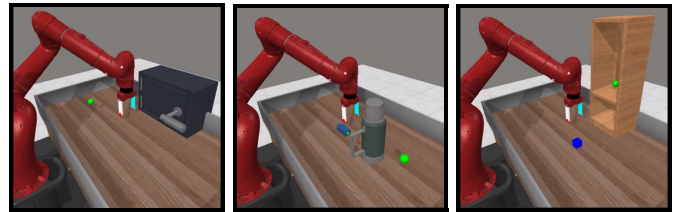
3) *Hyperparameters and model architecture:* The complete implementation details and configuration files are available in our official repository. The key details are summarized in Table II.

### B. Metaworld Tasks

For all Metaworld [78, 45] tasks, use the implementation provided by Cadene et al. [10]. We now provide a brief description of the tasks, however we recommend the interested reader to consult [78, 45] for the complete details.

#### 1) Task Description:

- **Door open** (door-open-v3). The robot must open a door with a revolving joint. The door positions are randomized.
- **Stick push** (stick-push-v3). The robot must grasp a stick and push a box using the stick. The stick positions are randomized.
- **Shelf place** (shelf-place-v3). The robot must pick and place a puck onto a shelf. The puck and shelf positions are randomized.



(a) Door open      (b) Stick push      (c) Shelf place

Fig. 9: Scene visualization of the 3 Metaworld tasks.

All goal positions are randomized as well.

2) *Dataset Description:* The datasets contain 50 demonstrations; however Yu et al. [78], McLean et al. [45] do not disclose how the data was collected.

Category	Hyperparameter	can	square	transport
Policy	Policy type	RNN-based behavior cloning (BC-RNN)	Diffusion policy based on Chi et al. [14]	Diffusion policy based on Chi et al. [14]
Policy	Batch size	16	16	16
Policy	Number of steps	100,000	100,000	200,000
Optimizer & LR	Optimizer	Adam	AdamW	AdamW
Optimizer & LR	Base learning rate	1e-4	1e-4	1e-4
Optimizer & LR	Weight decay (L2)	0.0	1e-6	1e-6
Optimizer & LR	LR scheduler type	multistep	cosine	cosine
Optimizer & LR	Scheduler cycles	—	0.5	0.5
Optimizer & LR	Scheduler epochs	none (constant LR, empty schedule)	—	—
Optimizer & LR	Warmup steps	0 (no warmup)	500	500
Diffusion (DDPM)	UNET enabled	—	true	true
Diffusion (DDPM)	UNET down dims	—	[256, 512, 1024]	[256, 512, 1024]
Diffusion (DDPM)	UNET kernel size	—	5	5
Diffusion (DDPM)	UNET group norm groups	—	8	8
Diffusion (DDPM)	Diffusion step embed dim	—	256	256
Diffusion (DDPM)	EMA enabled	—	true	true
Diffusion (DDPM)	EMA power	—	0.75	0.75
Diffusion (DDPM)	DDPM enabled	—	true	true
Diffusion (DDPM)	DDPM train timesteps	—	100	100
Diffusion (DDPM)	DDPM inference timesteps	—	100	100
Diffusion (DDPM)	Beta schedule	—	squaredcos_cap_v2	squaredcos_cap_v2
Diffusion (DDPM)	Prediction type	—	epsilon (noise prediction)	epsilon (noise prediction)
Diffusion (DDPM)	Clip sample	—	true	true
Diffusion (DDPM)	DDIM enabled	—	false	false
RNN Policy (BC-RNN)	RNN enabled	true	—	—
RNN Policy (BC-RNN)	RNN type	LSTM	—	—
RNN Policy (BC-RNN)	RNN hidden dim	1000	—	—
RNN Policy (BC-RNN)	RNN num layers	2	—	—
RNN Policy (BC-RNN)	RNN horizon	10	—	—
RNN Policy (BC-RNN)	RNN bidirectional	false	—	—
RNN Policy (BC-RNN)	Output distribution	GMM (mixture of Gaussians)	—	—
RNN Policy (BC-RNN)	GMM enabled	true	—	—
RNN Policy (BC-RNN)	GMM num modes	5	—	—
RNN Policy (BC-RNN)	GMM min std	1e-4	—	—
RNN Policy (BC-RNN)	GMM std activation	softmax	—	—
RNN Policy (BC-RNN)	GMM low-noise eval	true	—	—
RNN Policy (BC-RNN)	Gaussian head	disabled	—	—
RNN Policy (BC-RNN)	VAE	disabled	—	—
RNN Policy (BC-RNN)	Transformer	disabled	—	—
Rollout / Evaluation	Rollout episodes	50	50	50
Rollout / Evaluation	Rollout horizon	400	400	1100
Rollout / Evaluation	Rollout and checkpoint rate	5000 steps	5000 steps	10000 steps

TABLE II: Hyperparameters and model settings for the Robomimic tasks.

3) *Hyperparameters and model architecture*: The complete implementation details and configuration files are available in our official repository. The key details are summarized in Table III. All tasks use the same configuration.

### C. Real Tasks

All real tasks we use the official lerobot library [10]. We now provide a brief description of the tasks.

#### 1) Task Description:

- **Drawer open.** The robot must open a drawer by pulling a handle. The position of the drawer is fixed for all episodes; however, 5 different lighting conditions were used.
- **Pick and place marker.** The robot must pick up a marker and then drop into a pen holder. The position of the pen holder and marker are independently sampled from a fixed set of 7 locations (2 novel location were used that were not preset during the recording of the dataset).
- **Organize objects.** If a marker/pen is placed on the table, the robot must place it on a book, else if a charging brick is placed on the table, the robot must (1) first open a drawer, (2) then place the brick in the drawer, (3) and finally then close the drawer. The position of the drawer is fixed for all episodes. The position of the charging brick, marker and book are sampled from a fixed set of 5 random positions. There are no episodes where both the marker and the charging brick are placed on the table.
- **Mug Drag.** The robot must grasp a hook and drag a mug to a square goal region by using the hook as an intermediate tool. The position of the hook is randomized and the position of the mug is always to the left of the goal, however the distance to the goal is randomized.



Fig. 10: Scene visualization of the drawer open task, pick and place marker task and mug drag task.

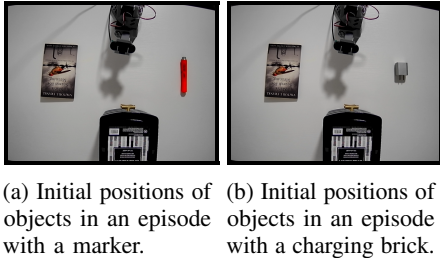


Fig. 11: Scene visualization of the organize objects tasks.

2) *Dataset Description*: The drawer open and Pick and place marker datasets contain 50 demonstrations, whereas the organize objects and mug drag datasets contains 100 demonstrations collected by a single experienced teleoperator. The pick and place marker and mug drag tasks use two cameras: one mounted on the robot’s wrist and another mounted above the workspace providing a top-down view. The drawer opening and object organization tasks use an additional camera with a diagonal side view. All cameras capture plain RGB images at 30 FPS with a resolution of 480 (height) by 640 (width) pixels.

3) *Hyperparameters and model architecture*: We use the same configuration and setup as in Table III, with the only change being batch size set to 64, training steps set to 60000 steps and rollout rate every 20000 steps.

## APPENDIX G ADDITIONAL RESULTS

### A. Additional Results for Section VII

Table IV provides the complete and full results for metaworld experiments that were summarized in Figure 5.

Table V provides the complete and full results for robomimic experiments that were summarized in Figure 3.

### B. Additional Results for Section VIII

Figure 12 shows the effect of the number of signature levels on the success rate for the Can task.

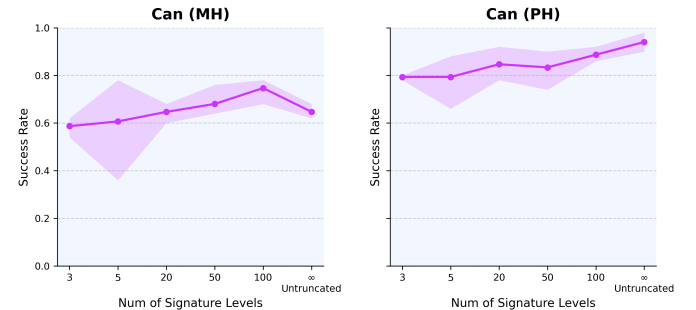


Fig. 12: Number of signature levels vs. success rate results. Results are averaged over three random seeds, and the error bars indicate the minimum and maximum values. Parameters (such as dataset size) are set to  $m = 120$  and  $p = 0$ .

### C. Additional results for low-dimensional representation method

In this subsection, we provide a limited evaluation of the low-dimensional representation method discussed in Appendix A. Conveniently, Robomimic already supplies low-dimensional observations for each task in its low-dim datasets, which we use for our analysis. The results are as follows.

Category	Hyperparameter	Value
Model + Architecture	Model type	smolvla [69]
	Vision–language backbone	HuggingFaceTB/SmolVLM2-500M-Video-Instruct
	VLM transformer layers	16 transformer layers from the VLM stack
	Number of expert layers	0 (expert interleaved into VLM stack; only expert is trained)
	Expert width multiplier	0.75 (expert MLP width vs. VLM width)
	Attention mode	cross-attn w/ periodic self-attn
	Self-attention frequency	Self-attention every 2 layers
	KV cache for inference	Enabled
Training / Finetuning behaviour	Vision encoder frozen	true
	Train expert head only	true (only expert + small heads get gradients)
	Train state projection MLP	true
	Load pretrained VLM weights	true (loads pretrained SmolVLM2 weights)
	Image special tokens	false
Optimizer & LR schedule	Optimizer	AdamW (from LeRobot training utilities)
	Base learning rate	$1 \times 10^{-4}$ peak learning rate
	Adam betas	(0.9, 0.95)
	Adam epsilon	$1 \times 10^{-8}$
	Weight decay	$1 \times 10^{-10}$ (very light weight decay)
	Gradient clipping norm	10 (global grad clipping)
	LR scheduler type	Cosine decay with warmup
	Warmup steps	1000 warmup steps
	Decay steps	30000 cosine decay steps
	Minimum learning rate	$2.5 \times 10^{-6}$ (minimum LR plateau)
Overrides from training command	Batch size	8
	Number of training steps	40000
Rollout / Evaluation	Rollout episodes	50
	Rollout horizon	400
	Rollout and checkpoint rate	2000 steps

TABLE III: SmolVLA hyperparameters and training configuration for the Metworld tasks.

Task	Method	Num. of Demos.	Seed 1	Seed 2	Seed 3	Mean	Min	Max
Door open	FAKTUAL	25	0.72	0.60	0.74	0.69	0.60	0.74
	random	25	0.62	0.52	0.66	0.60	0.52	0.66
	FAKTUAL	35	0.66	0.62	0.74	0.67	0.62	0.74
	random	35	0.70	0.56	0.78	0.68	0.56	0.78
	FAKTUAL	45	0.68	0.64	0.68	0.67	0.64	0.68
	random	45	0.72	0.50	0.86	0.69	0.50	0.86
Shelf place	full dataset	50	0.68	0.56	0.76	0.67	0.56	0.76
	FAKTUAL	25	0.12	0.08	0.08	0.09	0.08	0.12
	random	25	0.08	0.04	0.08	0.07	0.04	0.08
	FAKTUAL	35	0.12	0.08	0.10	0.10	0.08	0.12
	random	35	0.10	0.08	0.08	0.09	0.08	0.10
	FAKTUAL	45	0.12	0.06	0.08	0.09	0.06	0.12
Stick push	random	45	0.10	0.04	0.10	0.08	0.04	0.10
	full dataset	50	0.06	0.04	0.08	0.06	0.04	0.08
	FAKTUAL	25	0.44	0.26	0.22	0.29	0.18	0.44
	random	25	0.42	0.16	0.18	0.27	0.16	0.42
	FAKTUAL	35	0.46	0.26	0.20	0.30	0.18	0.46
	random	35	0.42	0.16	0.20	0.27	0.16	0.42
Stick push	FAKTUAL	45	0.46	0.20	0.18	0.28	0.18	0.46
	random	45	0.42	0.18	0.22	0.27	0.18	0.42
	full dataset	50	0.46	0.16	0.16	0.26	0.16	0.46

TABLE IV: Success rates for all metaworld manipulation tasks over 3 seeds. Mean, minimum, and maximum are computed across seeds.

Task	Method	Num. of Demos.	Seed 1	Seed 2	Seed 3	Mean	Min	Max	
Can (MH)	FAKTUAL	60	0.72	0.80	0.70	0.74	0.70	0.80	
	random	60	0.62	0.72	0.76	0.70	0.62	0.76	
	FAKTUAL	120	0.82	0.88	0.68	0.79	0.68	0.88	
	random	120	0.76	0.70	0.78	0.75	0.70	0.78	
	FAKTUAL	180	0.76	0.80	0.74	0.77	0.74	0.80	
	random	180	0.70	0.74	0.78	0.74	0.70	0.78	
	FAKTUAL	240	0.82	0.86	0.80	0.83	0.80	0.86	
	random	240	0.78	0.52	0.86	0.72	0.52	0.86	
	full dataset	280	0.80	0.74	0.84	0.79	0.74	0.84	
Can (PH)	FAKTUAL	30	0.76	0.82	0.70	0.76	0.70	0.82	
	random	30	0.58	0.66	0.66	0.63	0.58	0.66	
	FAKTUAL	60	0.86	0.90	0.76	0.84	0.76	0.90	
	random	60	0.76	0.78	0.70	0.75	0.70	0.78	
	FAKTUAL	90	0.84	0.92	0.86	0.87	0.84	0.92	
	random	90	0.90	0.82	0.80	0.84	0.80	0.90	
	FAKTUAL	120	0.98	0.98	0.90	0.95	0.90	0.98	
	random	120	0.88	0.82	0.88	0.86	0.82	0.88	
	FAKTUAL	150	0.94	0.88	0.94	0.92	0.88	0.94	
	random	150	0.80	0.90	0.72	0.81	0.72	0.90	
		full dataset	180	0.86	0.88	0.96	0.90	0.86	0.96
	Square (MH)	FAKTUAL	60	0.28	0.26	0.30	0.28	0.26	0.30
random		60	0.30	0.26	0.32	0.29	0.26	0.32	
FAKTUAL		120	0.46	0.50	0.44	0.47	0.44	0.50	
random		120	0.44	0.48	0.44	0.45	0.44	0.48	
FAKTUAL		180	0.56	0.60	0.54	0.57	0.54	0.60	
random		180	0.54	0.52	0.54	0.53	0.52	0.54	
FAKTUAL		240	0.62	0.64	0.66	0.64	0.62	0.66	
random		240	0.62	0.56	0.60	0.59	0.56	0.62	
	full dataset	280	0.60	0.56	0.62	0.59	0.56	0.62	
Square (PH)	FAKTUAL	30	0.20	0.24	0.20	0.21	0.20	0.24	
	random	30	0.22	0.22	0.30	0.25	0.22	0.30	
	FAKTUAL	60	0.48	0.48	0.46	0.47	0.46	0.48	
	random	60	0.48	0.58	0.58	0.55	0.48	0.58	
	FAKTUAL	90	0.64	0.66	0.70	0.67	0.64	0.70	
	random	90	0.64	0.64	0.54	0.61	0.54	0.64	
	FAKTUAL	120	0.76	0.76	0.72	0.75	0.72	0.76	
	random	120	0.74	0.72	0.72	0.73	0.72	0.74	
	FAKTUAL	150	0.78	0.78	0.80	0.79	0.78	0.80	
	random	150	0.76	0.74	0.76	0.75	0.74	0.76	
		full dataset	180	0.78	0.74	0.78	0.77	0.74	0.78
	Transport (MH)	FAKTUAL	60	0.08	0.08	0.08	0.08	0.08	0.08
random		60	0.14	0.04	0.08	0.09	0.04	0.14	
FAKTUAL		120	0.14	0.10	0.10	0.11	0.10	0.14	
random		120	0.12	0.10	0.06	0.09	0.06	0.12	
FAKTUAL		180	0.16	0.14	0.12	0.14	0.12	0.16	
random		180	0.16	0.16	0.16	0.16	0.16	0.16	
FAKTUAL		240	0.26	0.14	0.20	0.20	0.14	0.26	
random		240	0.22	0.08	0.18	0.16	0.08	0.22	
	full dataset	280	0.20	0.14	0.16	0.17	0.14	0.20	

TABLE V: Success rates for all robomimic manipulation tasks over 3 seeds. Mean, minimum, and maximum are computed across seeds.

Task	Curated Dataset	Success rate (%)
Can (PH)	Full dataset (180 episodes)	84 ± 4
	Random (90 episodes)	68 ± 7
	Our method (90 episodes)	86 ± 3
Can (MH)	Full dataset (270 episodes)	74 ± 6
	Random (120 episodes)	62 ± 2
	Our method (120 episodes)	74 ± 7

TABLE VI: Robomimic low dim results. We used vanilla BC, BC with RNN achieves a 100% success rate providing no meaningful insight.

## APPENDIX H RELATED WORKS COVERING DATASET DIVERSITY IN GENERAL ML

### a) Measuring Dataset Diversity in Machine Learning:

Several commonly used diversity metrics depend on a reference distribution or dataset, characterize diversity in terms of how well the reference is covered [72, 28, 16, 57, 61, 47]. Other existing metrics assess diversity using a pre-trained classifier, and thus require access to labeled datasets [62, 71]. There are proposed metrics [56, 67, 6] that use similarity scores to define diversity, such similarity scores can include average

pairwise similarity score or the complement, the average dissimilarity. However, all these methods exhibit drawbacks, such as requiring a reference distribution, relying on manual inspection of samples, or failing to account for correlations between different features. Friedman and Dieng [23] addresses many of these challenges by introducing the Vendi Score, a principled metric for quantifying dataset diversity. The Vendi score has found several useful extensions throughout computer science for: measuring functional diversity [19], improving retrieval augmented generation [58], and measuring information gain [50]. We extend the ideas underlying the Vendi Score to the robotics domain.

b) *Effect of Dataset Diversity on Model Performance in Machine Learning:* Yu et al. [79] show that the diversification of training samples alleviates overfitting and improves model generalization and accuracy in natural language processing. In an imaging-through-scattering setting, Zhang et al. [80] show that increasing the diversity of the training dataset improves the deep neural network's ability to approximate the underlying linear physical mapping, thereby enabling robust generalization to unseen datasets. Jung et al. [33] use a Vendi-style entropy, G-Vendi. They show that G-Vendi strongly correlates with how a (reasoning) model performs in unseen distributions when trained on that dataset.

#### APPENDIX I PROOFS

**Lemma 1.** *Consider the setting from Definitions 3 & 4. Then*

$$H_{\text{von neumann}}^{\text{sig}}(d_1, d_2, \dots, d_n) = H_{\text{shannon}}^{\text{sig}}(d_1, d_2, \dots, d_n).$$

*Proof:* Consider the signature kernel matrix  $K^{\text{sig}}$  from Definition 3. Since the signature kernel matrix  $K^{\text{sig}}$  is positive semidefinite and diagonalizable, it has an eigendecomposition of the form  $H \text{diag}(\lambda_1, \dots, \lambda_n) H^{-1}$ . Then  $\ln K^{\text{sig}} = H \text{diag}(\ln \lambda_1, \dots, \ln \lambda_n) H^{-1}$ . Trivially,  $\text{Tr}(H \text{diag}(\lambda_1, \dots, \lambda_n) H^{-1}) = \text{Tr}(\text{diag}(\lambda_1, \dots, \lambda_n))$  because the trace is similarity-invariant. Then we have,

$$\begin{aligned} \text{Tr}\left(\frac{K^{\text{sig}}}{n} \ln \frac{K^{\text{sig}}}{n}\right) &= \text{Tr}\left(H \text{diag}(\lambda_1, \dots, \lambda_n) H^{-1} \right. \\ &\quad \left. \ln(H \text{diag}(\lambda_1, \dots, \lambda_n) H^{-1})\right) \\ &= \text{Tr}\left(H \text{diag}(\lambda_1, \dots, \lambda_n) H^{-1} \right. \\ &\quad \left. H \text{diag}(\ln \lambda_1, \dots, \ln \lambda_n) H^{-1}\right) \\ &= \text{Tr}\left(\text{diag}(\lambda_1, \dots, \lambda_n) \text{diag}(\ln \lambda_1, \dots, \ln \lambda_n)\right) \\ &= \sum_{i=1}^n \lambda_i \ln \lambda_i. \end{aligned}$$

Hence,

$$\begin{aligned} H_{\text{von neumann}}^{\text{sig}}(d_1, d_2, \dots, d_n) &= -\text{Tr}\left(\frac{K^{\text{sig}}}{n} \ln \frac{K^{\text{sig}}}{n}\right) \\ &= -\sum_{i=1}^n \lambda_i \ln \lambda_i \\ &= H_{\text{shannon}}^{\text{sig}}(d_1, d_2, \dots, d_n). \end{aligned}$$